1-1-2017

Elucidating Structure, Function, And Small Molecular Interactions Of Human Immunodeficiency Virus And Chikungunya Virus

Kristin Nicole Slater
Wayne State University,

ELUCIDATING STRUCTURE, FUNCTION, AND SMALL MOLECULE INTERACTIONS OF HUMAN IMMUNODEFICIENCY VIRUS AND CHIKUNGUNYA VIRUS

by

KRISTIN NICOLE SLATER

THESIS

Submitted to the Graduate School

of Wayne State University

Detroit, Michigan

in partial fulfillment of the requirements

for the degree of

MASTER OF SCIENCE

2017

MAJOR: BIOCHEMISTRY AND MOLECULAR BIOLOGY

Approved by:

Advisor	Date
Committee Member	Date
Committee Member	Date

ACKNOWLEDGEMENTS

I want to thank Dr. Ladislau Kovari and Iulia Kovari for giving me the opportunity and reassurance needed to complete my masters. I am grateful for their guidance as well as the freedom to pursue new ideas. Their expertise has provided me the tools needed to effectively explore virology and drug design. I would also like to thank my lab members for training, encouraging, and working with me as a team on our projects. Additionally, I would like to thank Wayne State University School of Medicine for the resources needed to conduct my research.

TABLE OF CONTENTS

LIST OF FIGURES

Number *Page*

LIST OF TABLES

Number *Page*

Section 1: HIV-1 Multidrug Resistant Protease with Residue 28 Insertion

CHAPTER I: INTRODUCTION

1.1 HIV-1 Viral Background

Human immunodeficiency virus (HIV) is a positive-sense, enveloped *lentivirus* that infects CD4+ T cells and can lead to the development of acquired immune deficiency syndrome (AIDS) [2].

1.2 Clinical Background

The Center for Disease Control (CDC) estimates that 1.2 million people are living with HIV in the United States as of 2013 and about 36.7 million people worldwide as of June 2016 (CDC, 2016). HIV remains a worldwide concern as fatalities due to opportunistic infections continue to occur [3]. HIV is a retrovirus predominantly found as the HIV-1 strain [4, 5] . HIV-1 contains different viral proteins necessary for propagating its viral life cycle, one of which is the HIV-1 protease [6-9] .

1.3 Viral Mechanism/Protease Significance

HIV-1 protease (HIV-1 PR) is a 99 amino acid aspartyl protease that cleaves the Gag and Gag-pol polyproteins in 9 locations to release mature proteins required for new virion assembly [6, 7, 10-12]. The mechanism underlying the cleavage of the polyproteins is an almost symmetric interaction between the substrate and the catalytic aspartate residues from each monomer [13, 14].

1.4 Mutations/Insertions

Inhibiting the HIV-1 PR with one of nine FDA-approved protease inhibitors (PI) has proven to be a successful strategy to prevent viral maturation; however, drug resistance mutations in HIV-1 PR may act as a survival mechanism for the virus under pharmacologic pressure [15]. Multidrug

resistant mutations acquired by HIV-1 PR render conventional protease treatments less effective [12, 15-20], thus increasing the survival of the virus [12].

Insertion mutations are vastly underrepresented in the literature and their role remains unclear. We have recently identified a clinical isolate from the Wayne State University Infectious Disease Clinic in Detroit, MI which contains a five residue insertion between codons 28 and 29 of multidrug resistant HIV-1 protease.

1.5 Specific Aim

To study the effects of the five residue insertion on HIV-1 PR function, we created a homology model of the insertion mutant and submitted the model to a 40 ns molecular dynamics simulation.

CHAPTER II: MATERIAL AND METHODS

2.1 Phenotypic and Genotypic data

Phenotypic data for MDR28 was obtained by Phenosense® HIV drug resistance assay as performed at the Detroit Medical Center [21]. Genotypic data from the sequence of the mutant PR was provided by the Viroseq® HIV-1 genotyping system [22].

2.2 Homology Modeling

A homology model of multidrug resistant HIV-1 PR (MDR) containing a five amino acid insertion, Asp-Asp-Thr-Ile-Leu (DDTIL), immediately to the c-terminal side of the 28th residue (MDR28) was created using SWISS-MODEL [23-26]. A wild-type (WT) HIV-1 PR crystal structure, 2O4S.pdb was obtained from the RCSB protein data bank and used as a template for the MDR28 homology model [27]. A homology model for MDR without the insertion was made using the same template (2O4S.pdb). The crystal structure 2O4S was used as a WT control. The resulting homology model for the MDR28 was a homodimer containing a total of 208 amino acids. The WT and MDR models each contained 198 amino acids. All of the models were subjected to 40ns molecular dynamics(MD) simulations.

2.3 Molecular Dynamics Simulations

2.3.1 Protease Complex Preparation

Visual Molecular Dynamics (VMD) software (VMD v.1.9.2) [27] was used to prepare the systems for MD simulations. WT, MDR, and MDR28 were prepared without a peptide (apo) resulting in three systems, respectively.

2.3.2 System Preparation

The preparation of the system for the MD simulation was carried out using VMD software (VMD v.1.9.2) [28]. The PR complexes as well as the apo structures were placed in a 12 Å TIP3P water box and were then neutralized with 0.15 M $MgCl_2$. The simulations were performed for 40ns using NAMD (e) V 2.9. [29] and CHARMM force field 36 to set parameters [30] as previously described [31]. All simulations were run on the Wayne State University Grid (www.grid.wayne.edu).

2.4 Analysis

2.4.1 Structural Analysis

All structural analysis was carried out using VMD (VMD v1.9.2) [28]. Frame 17,000 was selected as a model frame for WT, MDR, and MDR28 out of the 20,000 frame simulation. This frame was chosen as it is located further into the simulation after the proteases have had time to adjust and stabilize.

RMSD values were calculated over the last 10 ns of the simulation using VMD (v 1.9.2). RMSF values were calculated for all 40 ns of the simulation. Secondary structural analysis was completed using the Ramachandran plot analysis tool. Ramachandran plots were used to analyze residues 23-42 of all three protease models for the last 10 ns of the simulation. RMSD model alignments of the full length PR, the hinge region, and the flap region were taken at 5 ns intervals of each PR RMSD. Model averages of MDR and MDR28 aligned with WT were also taken at 5 ns intervals throughout the simulation using the RMSD alignment tool in the PyMOL Molecular Graphics System (Version 1.8 Schrödinger, LLC).

CHAPTER III: RESULTS

3.1 Reduced replicative capacity and drug resistance of MDR28

In a Phenosense® susceptibility test, clinical isolate MDR28 displayed full or partial resistance to the following protease inhibitors (PIs): atazanavir (ATV/r), amprenavir (AMP/r), indinavir (IDV/r), tipranavir (TRV), and nelfinavir (NFV) (**Table 1**). Viroseq®, a genotypic antiretroviral drug resistance report was then performed, and MDR28 showed resistance mutations impacting the PIs IDV, LPV, fosamprenavir (FPV), and possible resistance to TPV, DRV, and ATV. Saquinavir (SQV) was the only inhibitor for which there were no known resistance mutations present (**Table 1**). A list of resistance mutations found

	ATV/r	DRV/r	FPV/r	IND/r	LPV	NFV	RTV	SQV/r	TPV/r
Phenotype	Resistant	Partially Susceptible	Resistant	Resistant	Partially Susceptible	Resistant	Resistant	Susceptible	Partially Susceptible
Genotype	Possible Resistance	Possible Resistance	Resistant	Resistant	Resistant	Resistant	N/A	Susceptible	Partially Susceptible

Table 1. Phenotypic and genotypic susceptibility data. Summary of phenotypic and genotypic resistance data provided by Phenosense® and Viroseq®.

Mutation	Requires additional mutation	Possible resistance	Resist
L10V	TPV,IDV,SQV,DRV,ATV,NFV,FPV	LPV	
V32I	TPV,IDV,LPV,DRV,ATV,NFV,FPV		
M46I	TPV, IDV,LPV,ATV,FPV	NFV	
I54L	IDV,SQV,LPV,DRV,ATV	NFV	FPV
A71V	TPV,IDV,SQV,LPV,ATV		

Table 2. MDR28 resistance mutations and corresponding PI resistance. Summary of Viroseq® HIV-1 genotype report with possible PI resistance profile.

in MDR28, and their contributions are available in **Tables 1 and 2**. Genotypic reports are more predictive of future drug resistance, and the phenotypic data can be predictive of the clinical outcome. It was also determined in a Phenosense® replicative capacity assay that in the absence of inhibitors the isolate MDR28 functioned at a reduced replicative capacity compared to WT (only 29% of WT) (**Figure 1**).

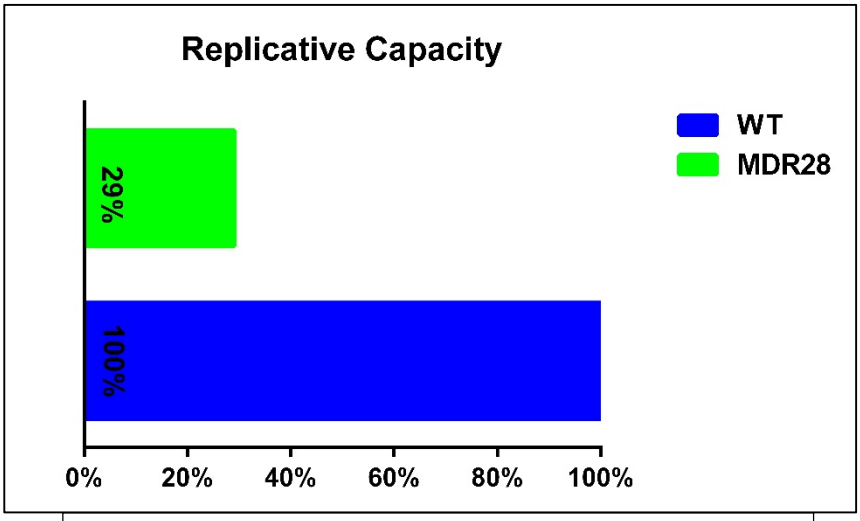

Figure 1. Replicative Capacity. Comparison of replicative capacity as percentage, visualized as a bar graph. MDR28 represented with green, WT represented with blue.

```
MDR28     PQITLWKRPVVTIKIGGQLKEALLDTGADDTILDDTILEEMSLPGRWKPKIIGGIGGFVK 60
WT        PQITLWKRPLVTIKIGGQLKEALLDTGADDT-----VLEEMSLPGRWKPKMIGGIGGFIK 55
MDR       PQITLWKRPVVTIKIGGQLKEALLDTGADDT-----ILEEMSLPGRWKPKIIGGIGGFVK 55
          *********:**********************     :*************:*******:*

MDR28     VRQYDQILIEICGHKVIGTVLVGPTPMNIIGRNLLTQIGC---- 100
WT        VRQYDQILIEICGHKAIGTVLVGPTPVNIIGRNLLTQIGCTLNF 99
MDR       VRQYDQILIEICGHKVIGTVLVGPTPMNIIGRNLLTQIGCTLNF 99
          ***************.**********:**************
```

Figure 2. Sequence alignment MDR28, WT, and MDR. The absence of an insertion is indicated by dashes (-), homology indicated with by the presence of an asterisk (*), mutations denoted by a colon (:).

3.2 Homology modeling of MDR28, WT, and MDR of MDR28, WT, and MDR:

Wildtype (WT) HIV-1 PR is a 99 amino acid aspartyl-protease. Two 99 amino acid monomers form a homodimer to create active HIV-1 PR. [7, 8, 11, 12]. In dimer form, both WT and multidrug resistant HIV-1 PR (MDR) contain 198 amino acids. MDR and the corresponding

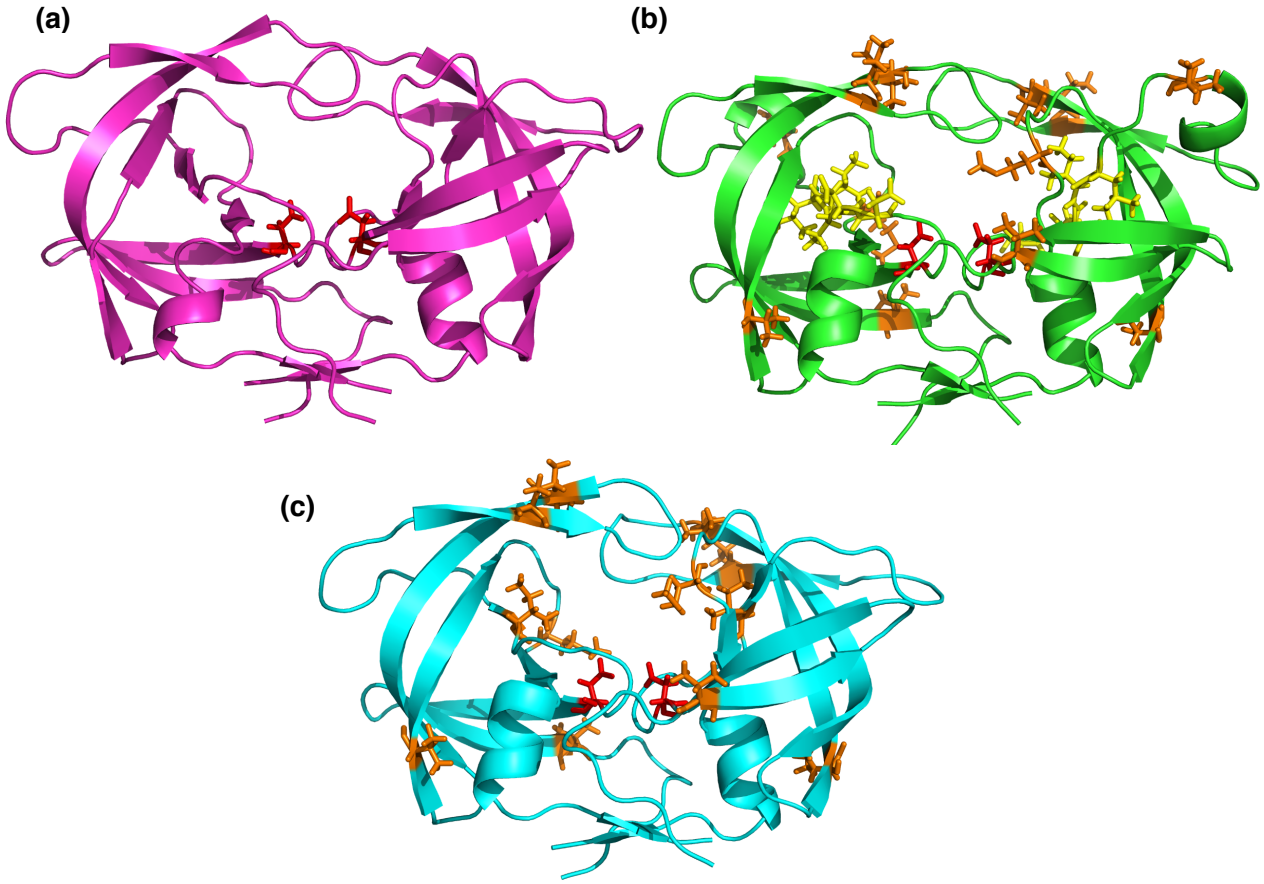

Figure 3. Ribbon representations of HIV-1 PR structures. (a) WT shown in magenta, catalytic asp25 in red **(b)** MDR28 shown in in green, multi-drug mutations in orange, asp25 in red, and insertion residues in yellow. **(c)** MDR shown in cyan with multidrug resistant mutations in orange and asp25 in red

homology model showed 6 mutations within each monomer sequence. These mutations are consistent in both MDR and our multidrug resistant HIV-1 PR (MDR28) isolate with an insertion immediately following the carboxyl terminus of amino acid 28. This added insertion results in a homodimer with 208 amino acids. (**Figure 1**)

The 5 residue insertion in MDR28 appears to promote the formation of an alpha helix in the hinge region that is not present in WT or MDR (**Figure 2**).The hinge region of the proteases are composed of amino acids 34-42 [2] , which normally affect the flap region and subsequent conformational ability [2]. The flap region is composed of residues 43-59 [2] and is responsible

for the proteases ability to take on an “open” or “closed” conformation, affecting its ability to bind to the substrate [11].

3.3 Secondary structure analysis

To determine whether the alpha helix in MDR28 was transient or present throughout the VMD simulation (VMD v.1.9.2) [28], the hinge regions of each model were analyzed with Ramachandran diagrams. Ramachandran diagrams plot phi vs. psi angles of the peptide linkages between amino acids, which compose the protease backbone [32]. Each data point represents one of 5,000 frames that were analyzed (materials and methods). Plots were generated of the insertion and the surrounding residues for each monomer (denoted as monomer A and monomer B) over the last 10 ns of the simulation. The MDR28 insertion residues were labeled 28a-28e (**Figure 5**). A change in secondary structure for MDR28 is consistent throughout the last 10ns of the simulation. Alpha helix formation is observed at residues 29-35 in MDR28, corresponding to residues 34-40 in WT and MDR (**Figure 6)**. No comparable secondary structure changes were seen in WT or MDR. No additional deviations in secondary structure were seen in surrounding residues. (**Figure 4, Figure 7**).

3.3.1 Prior to insertion

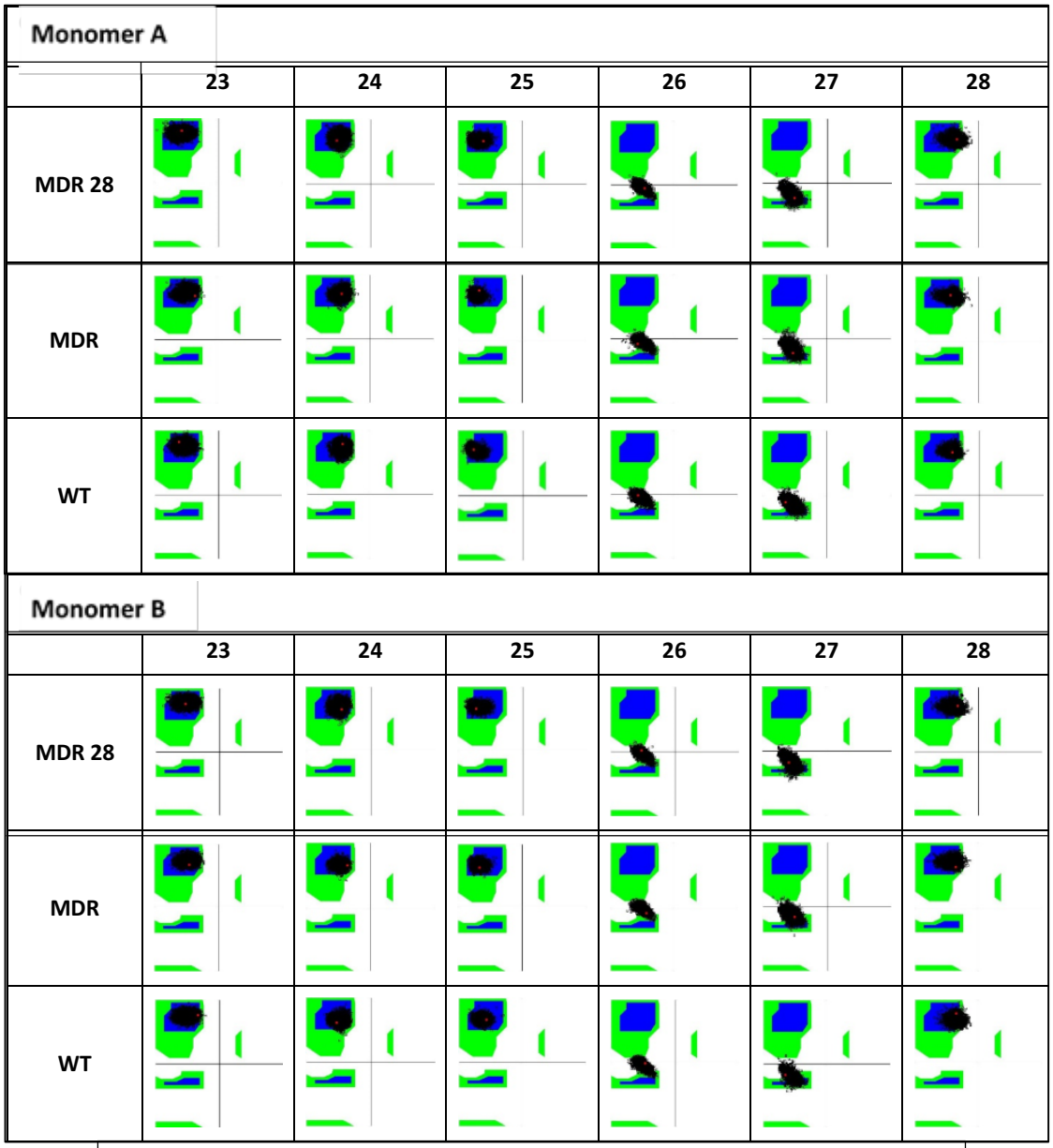

Figure 4. Ramachandran plots prior to insertion. MDR28, MDR, and WT residues 23-28 shown above. No obvious structural deviations noted.

3.3.2 Insertion residues

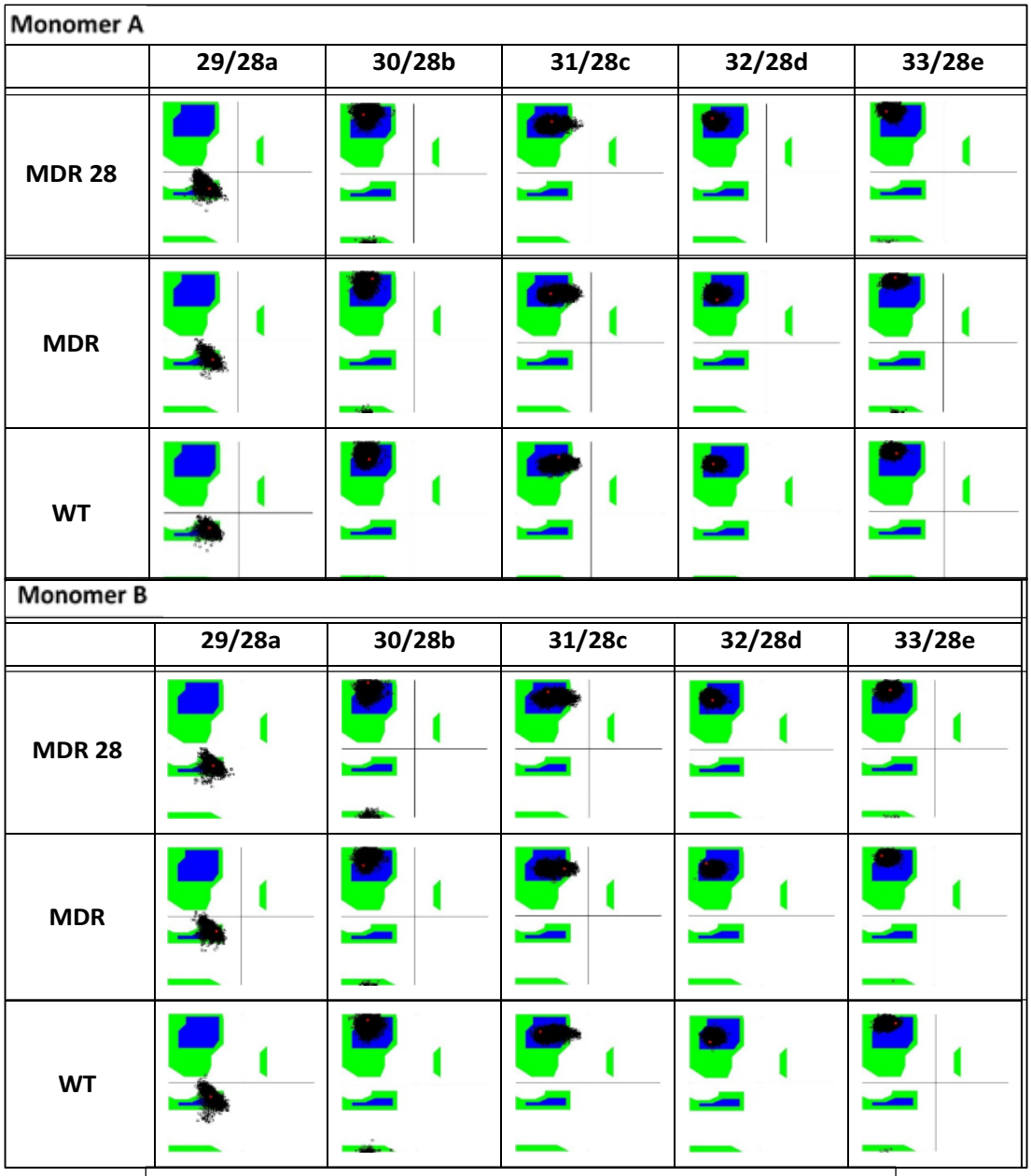

Figure 5. Ramachandran plots corresponding to insertion residues. MDR and WT residues 29-33, and MDR28 residues 28a-28e shown above. No obvious structural differences noted.

3.3.3 After insertion

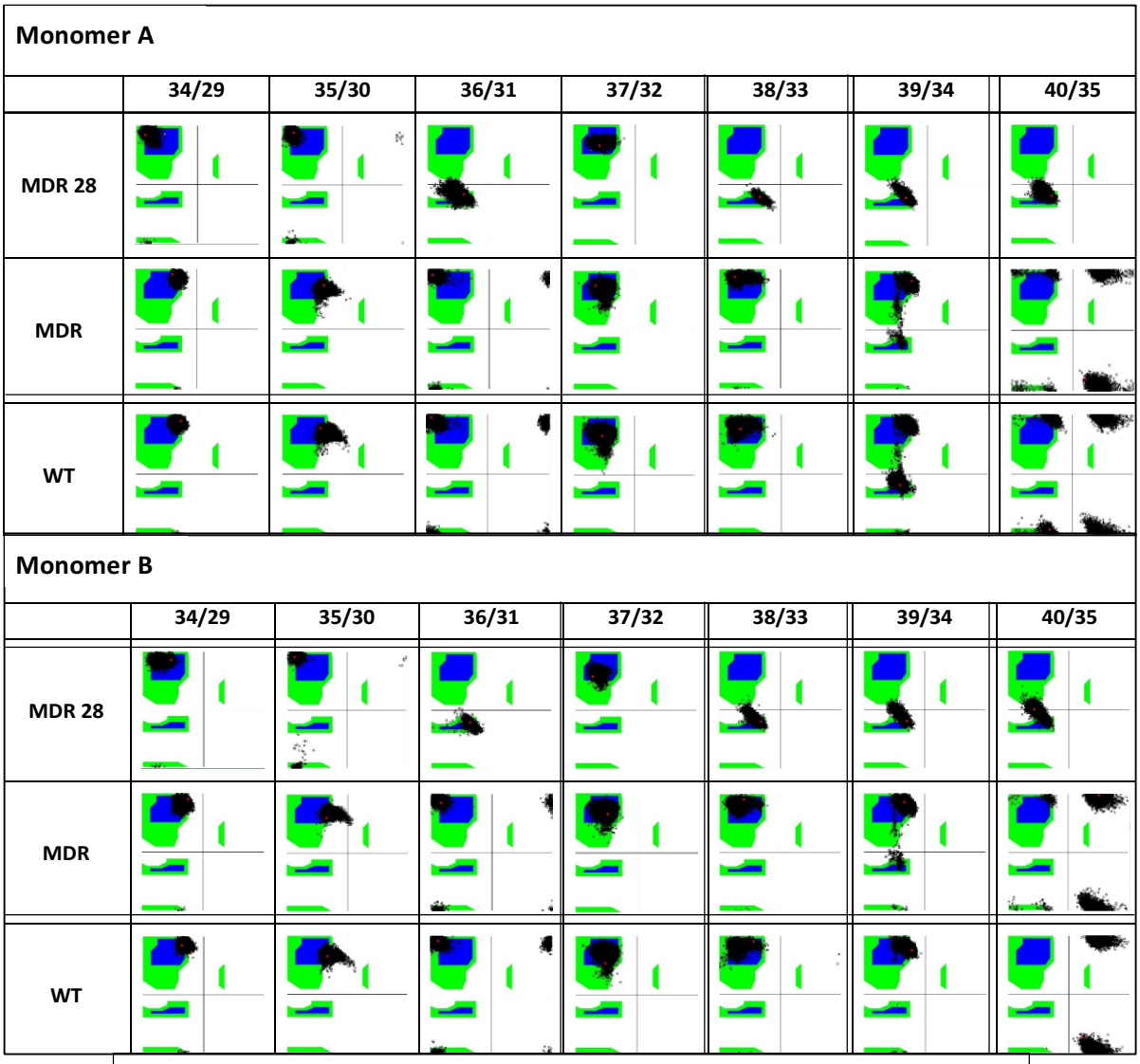

Figure 6. Ramachandran plots after insertion. WT and MDR residues 34-40, and MDR28 residues 29-35 shown above. Alpha helix formation observed in residues 31-35 of MDR28 only.

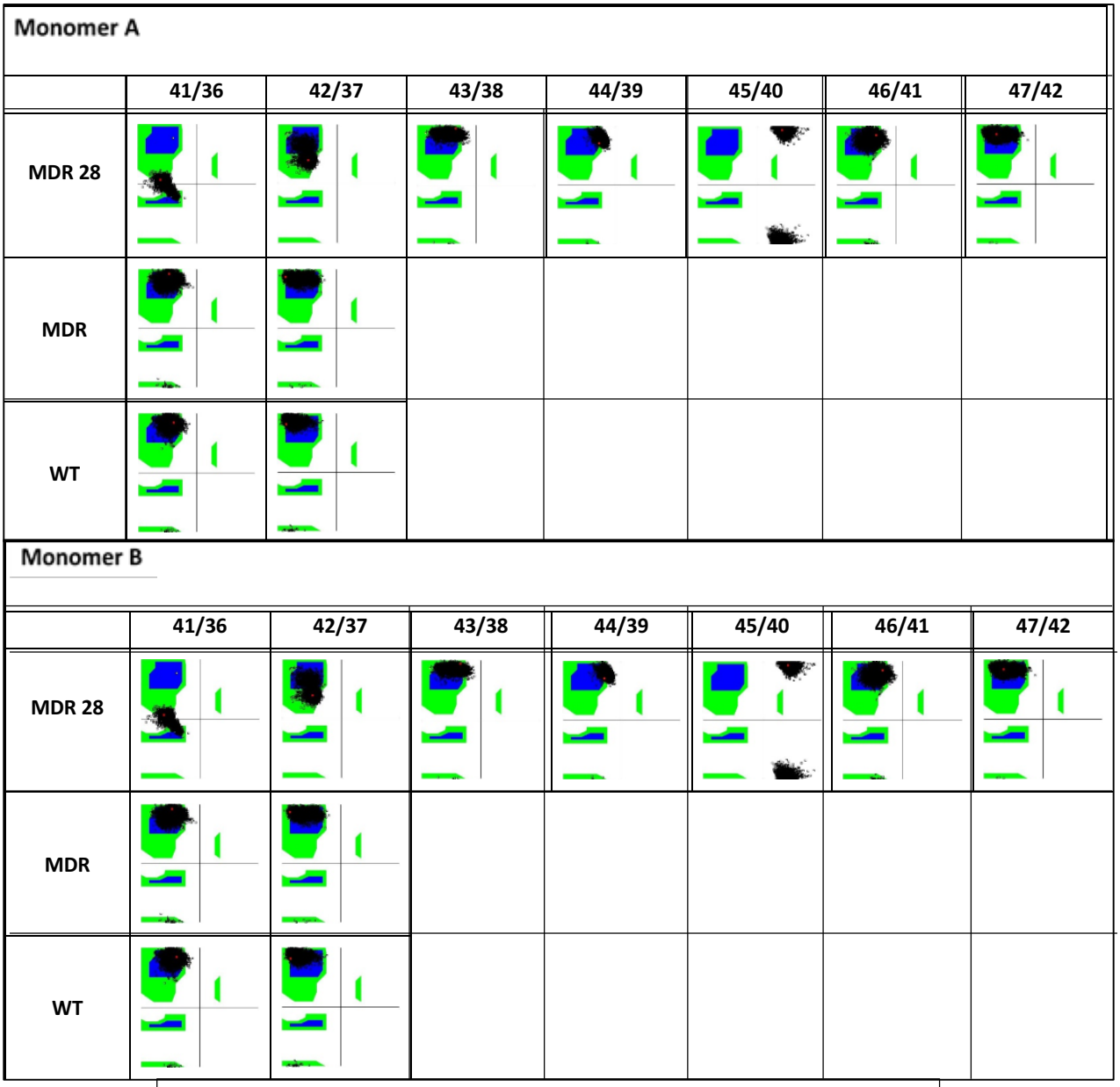

Figure 7. Ramachandran plots after insertion. MDR28, MDR, and WT residues following insertion. No obvious structural changes observed

3.4 Flexibility analysis through RMSF calculations

To determine if the addition of an alpha helix affected hinge and flap flexibility, RMSF was analyzed across the 40 ns simulation. The RMSF calculations were analyzed with VMD software (VMD v.1.9.2) [28]. Averages of the monomers of all three proteases— WT, MDR, and MDR28 were visualized as graphs (**Figure 8)** and models (**Figure 9**). No obvious changes in flexibility were noted. RMSF values were visualized for the hinge (**Figure 10**) and flap residues (**Figure 11**) to ensure no changes were seen. The RMSF analysis did not show substantial changes in flexibility between the proteases in any location.

3.4.1 RMSF averages of monomers

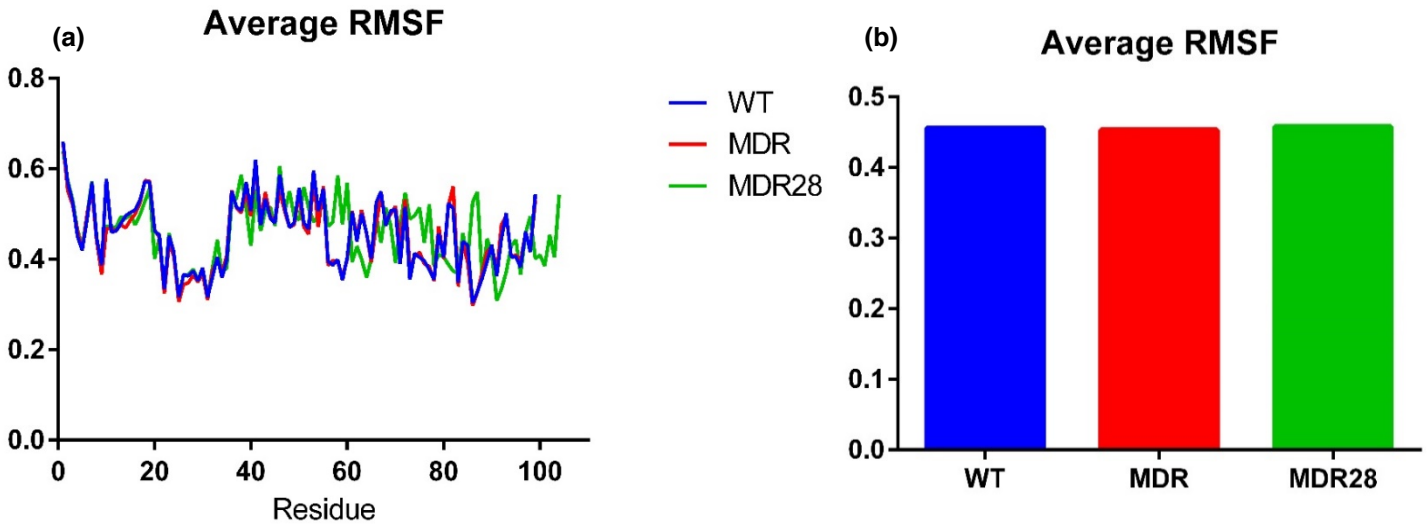

Figure 8. RMSF Averages of monomers. a) RMSF Averages represented as line graph with average RMSF vs residue. **b)** RMSF averages for all residues represented by bar graph

3.4.2 RMSF flexibility models

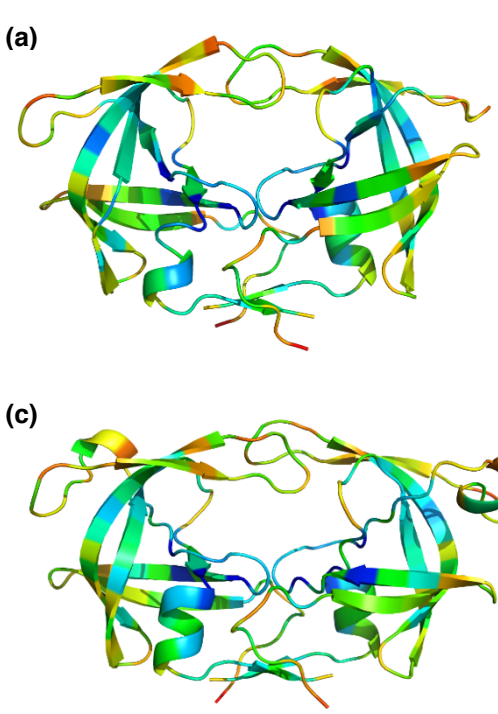

Figure 9. RMSF Represented by Model Highlighting. Red indicates a high degree of flexibility, blue indicates low degree of flexibility. **a)** WT **b)** MDR **c)** MDR28

3.4.3 RMSF averages hinge region

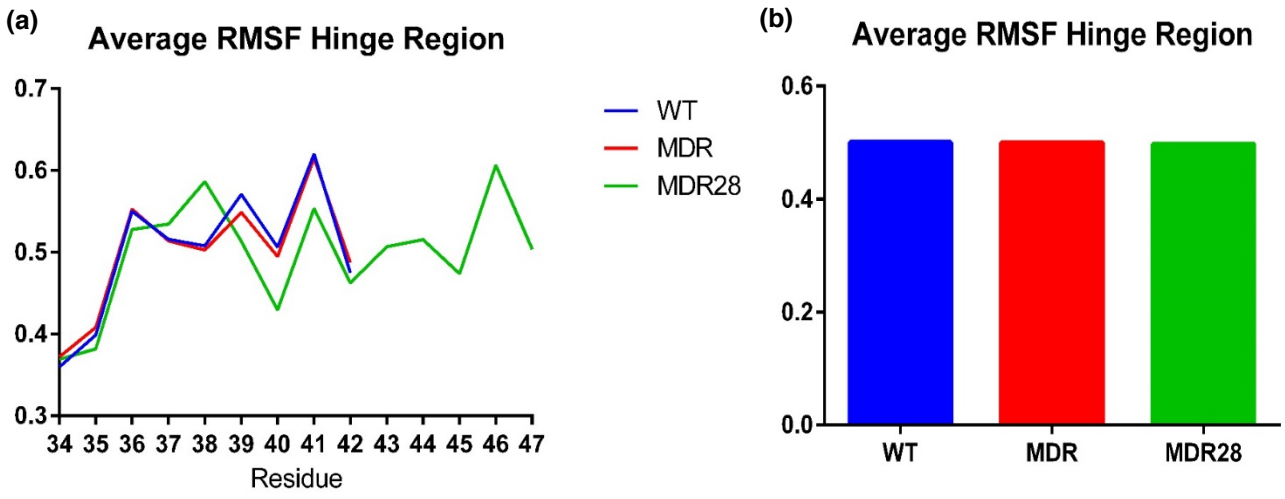

Figure 10. RMSF Averages Hinge Residues. a) RMSF hinge residues represented by RMSF vs Residue line graph **b)** RMSF hinge residues visualized as bar graph

3.4.4 RMSF flap region

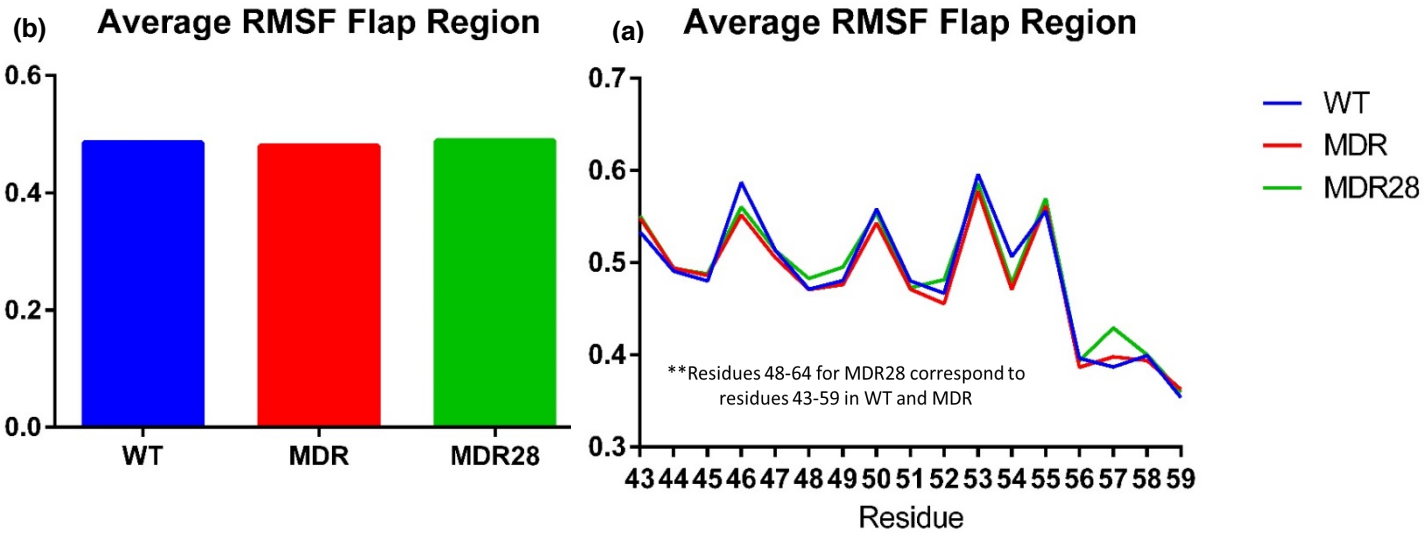

Figure 11. RMSF Averages Flap Residues. a) RMSF flap residues graphed as RMSF vs residue. **b)** RMSF flap residues visualized as a bar

3.5 RMSD analysis

Due to the presence of an alpha helix throughout the 40 ns simulation in MDR28, the effect of this structure on the flap and hinge dynamics were examined. RMSD analysis was calculated using VMD (VMD V.1.9.2.) [25] to determine whether the alpha helix altered the atomic coordinates in MDR28 compared to WT and MDR structures. Averaged RMSD values of each protease were taken and represented as line and bar graphs (**Figure 12**). In the hinge region, a peak is present at residue 39 of MDR28 (**Figure 13**). This deviation is not observed in WT or MDR. The flap residues were visualized using the same graphing methods (**Figure 14**). Comparatively, the dynamics of the flap region appear altered as well.

3.5.1 RMSD averages homodimers and monomers

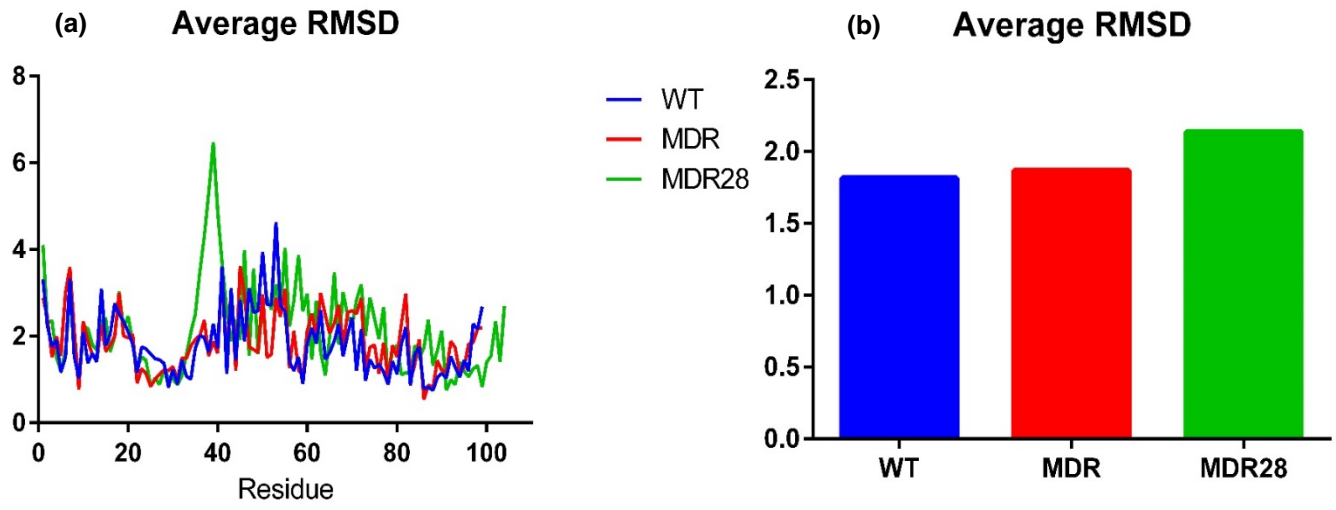

Figure 12. RMSD Averaged Monomer Values. a) Averaged monomer values represented as line graph (RMSD vs residue). **b)** Averaged residues visualized by bar graph

3.5.2 RMSD hinge region

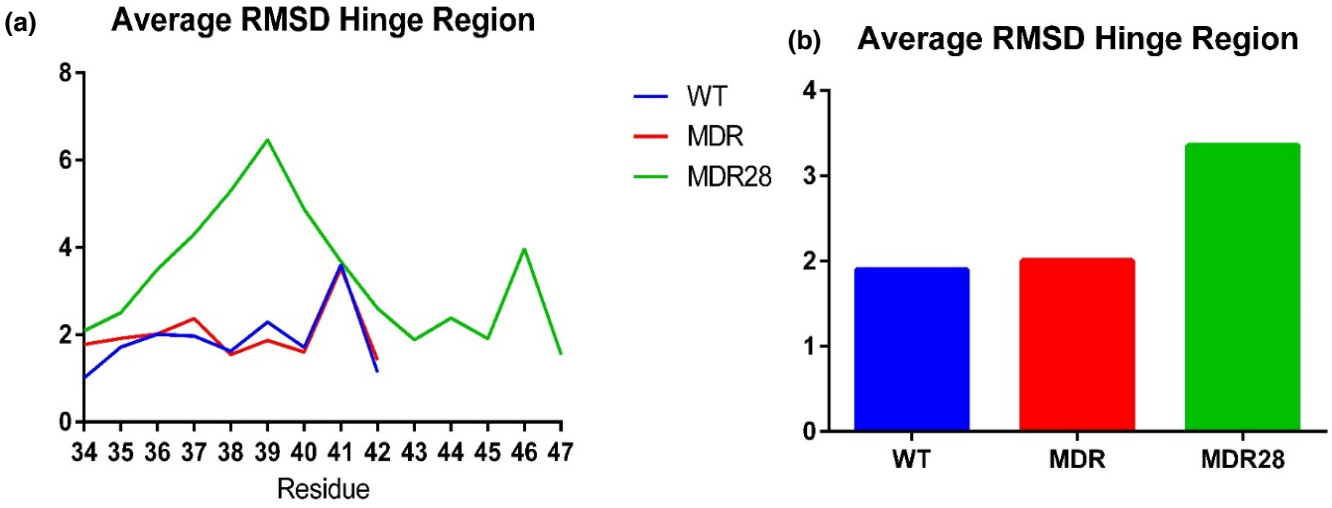

Figure 13. Average hinge region RMSD values. a) RMSD hinge averages for WT (blue), MDR (red), and MDR28 (green) represented by line graph (RMSD vs residue **b)** Averaged hinge region RMSD represented by bar graph

3.5.3 RMSD flap region

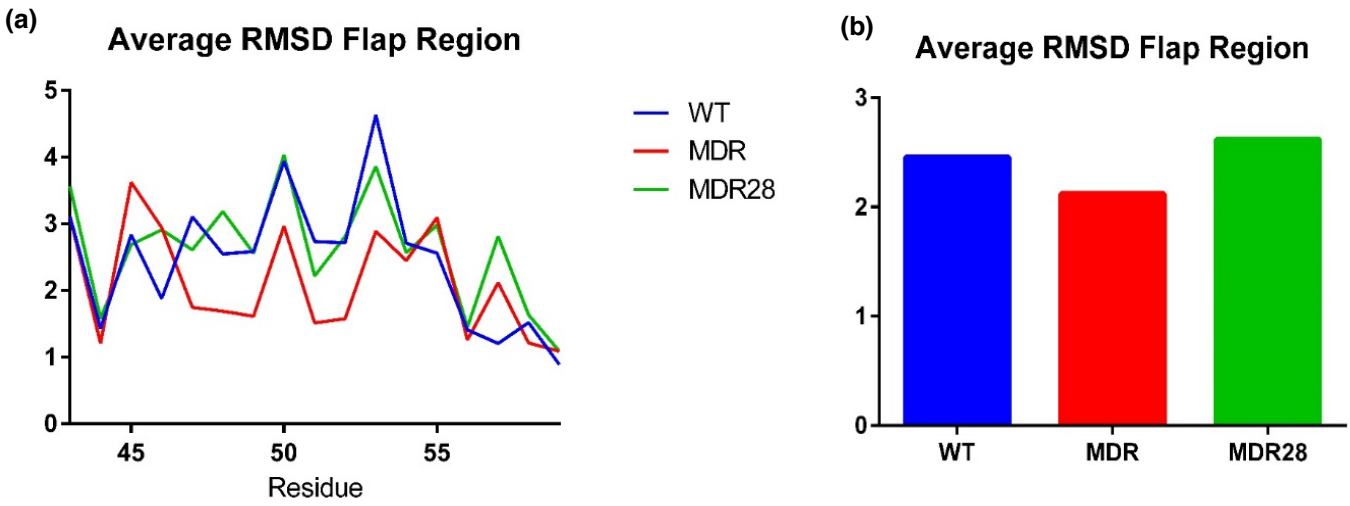

Figure 14. Average flap region RMSD values. a) RMSD flap region averages for WT (blue), MDR (red), and MDR28 (Green) represented by line graph (RMSD vs residue). **b)** Averaged flap region RMSD represented by bar graph

3.6 RMSD model analysis at 5 ns intervals suggests increased structural similarity:

To determine whether the dynamics information translated to similarities in structural alignment, RMSD values of MDR and MDR28 aligned with WT were taken at 5 ns intervals throughout the simulation. The model alignment values were measured using the RMSD alignment tool in the PyMOL Molecular Graphics System (Version 1.8 Schrödinger, LLC). The results suggest that over time MDR28 acts with increased structural similarity to WT. MDR28 consistently showed higher average similarity to WT in all three datasets—full length PR (**Figure 15**), hinge region (**Figure 16**), and flap region (**Figure 17**). The data for MDR and MDR28 were visualized using line graphs representing RMSD compared to WT vs time. Data averages for each region were visualized using bar graphs. The largest deviation in structural similarity between MDR and MDR28 when compared to WT, was seen between the flap regions (**Figure 17**), where MDR28 continued to show the highest amount of similarity to WT. The flap

region is imperative in accessibility to the active site, and subsequent substrate recognition and cleavage [33]. Furthermore, in previous studies mutant isolates were compared and those differing in only the insertions showed higher overall rates of replication [14]. MDR28 appears to compensate for MDR mutations by increasing structural similarity to WT. These results may indicate compensation to promote viral fitness as the underlying mechanism that promotes cleavage of the polyproteins. Subsequently, this would be dependent on proper structure and subsequent interactions between the substrate and the catalytic residue asp25 [13, 14].

3.6.1 RMSD full length model analysis:

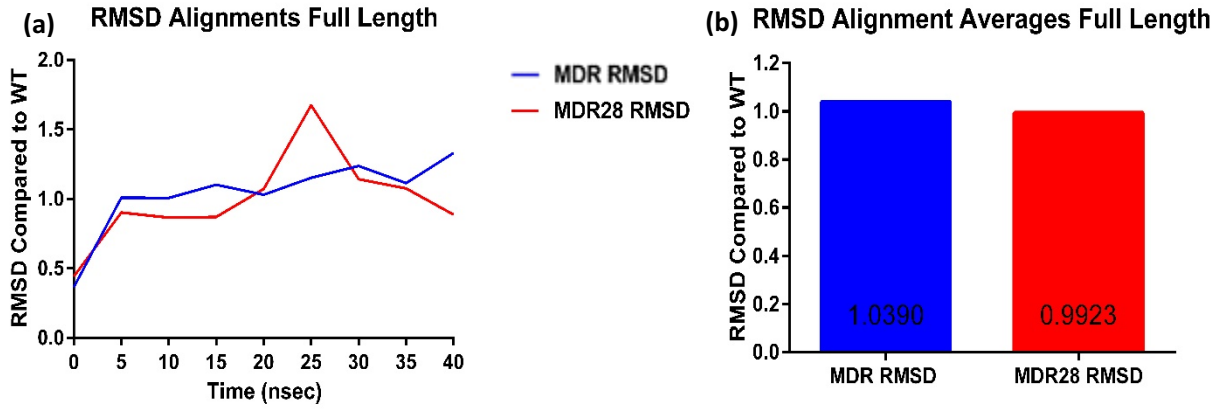

Figure 15. RMSD Model Alignment. a) RMSD PR alignments at 5 ns intervals visualized by line graph (RMSD compared to WT vs Time). **b)** RMSD Alignment PR averages visualized as bar graph.

3.6.2 RMSD hinge region model analysis:

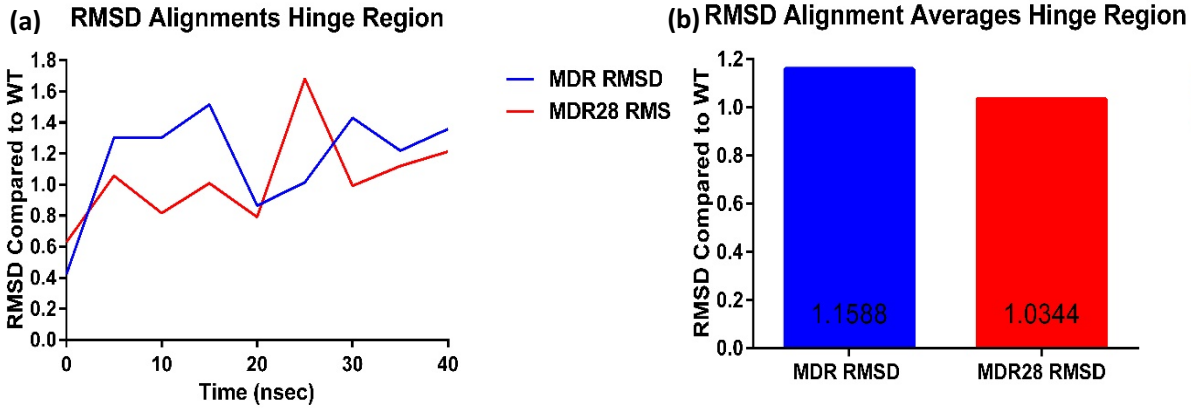

Figure 16. RMSD Model Alignment Hinge Region. a) RMSD hinge region alignments at 5 ns intervals visualized by line graph (RMSD compared to WT vs Time). **b)** RMSD Alignment hinge region averages visualized as bar graph.

3.6.3 RMSD flap region model analysis:

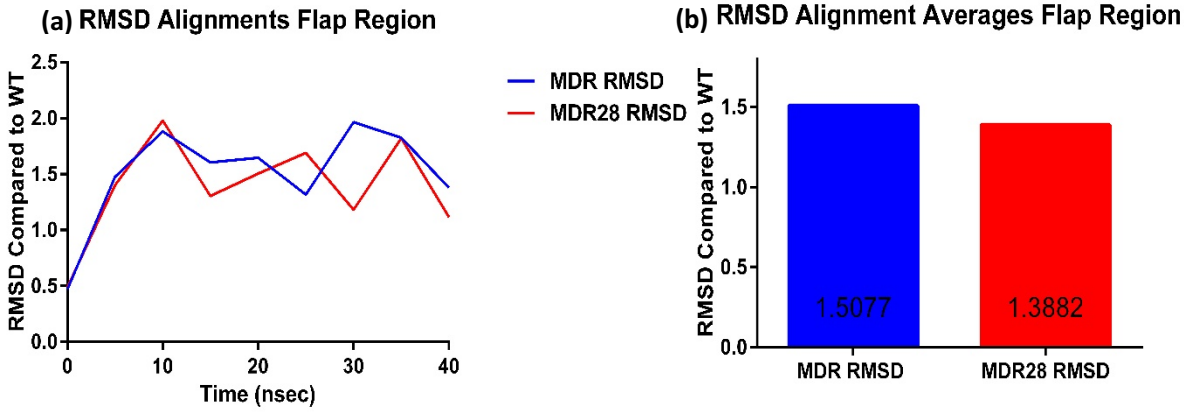

Figure 17. RMSD Model Alignment Flap Region. a) RMSD flap region alignments at 5 ns intervals visualized by line graph (RMSD compared to WT vs Time). **b)** RMSD Alignment flap region averages visualized as bar graph.

CHAPTER IV: CONCLUSION AND DISCUSSIONS

4.1 Overview

HIV is an incurable virus that accounts for many deaths in the US and worldwide as documented by the CDC (https://www.cdc.gov/hiv/basics/statistics.html). HIV often progresses to AIDS [6], which ultimately decreases lifespan via modes such as opportunistic infections [2]. HIV protease plays a crucial part in the viral life cycle [5, 6, 9-11] and without its ability to function the virus is incapable of completing replication [1, 33]. Though protease inhibitors have been effective in treating HIV infections [7, 9, 18, 34], HIV-1 PR has mutated as a potential means of preserving its viral life cycle [14]. Multidrug resistant HIV is caused by specific mutations [11, 35]. Additionally, strains of multidrug resistant HIV-1 are more difficult to treat [11, 14-19] potentially due to different intermolecular forces created by the changes in 6 key amino acids [36]. It has been suggested that insertions may compensate for resistance mutations, but little literature currently exists [14].

4.2 Key Findings

The insertion found in our clinical isolate created a shift in the protease structure, due to the addition of an alpha helix to the hinge region. This altered hinge region appears to act as a compensatory mechanism, reestablishing structural similarities to WT, which are necessary for efficient cleavage of viral polyproteins [13, 14]. The structural change is a likely contributor to the proteases ability to adopt “open” and “closed” conformations, as the hinge region is implicated in making conformational changes [18] by controlling the movement of the flap regions [10]. The flap residues are responsible for accessibility to the active site and subsequent substrate recognition and cleavage [33]. The change in hinge structure and dynamics resulted in a change in flap dynamics. The similarity in RMSD flap values for WT and MDR28 serves as

evidence of compensation and structural restoration. The insertion itself may be, in part, due to polymerase slippage [34] creating the consequential five amino acid repeat seen within the isolate. However, it is reasonable to think that the MDR28 hinge alteration is a viral adaptation as a means of promoting structural restoration, replicative capacity, and consequential viral fitness.

4.3 Concluding Remarks

Further studies will need to be conducted to decisively conclude the role of insertions in viral fitness.

Abstract

Human immunodeficiency virus-1 (HIV-1) is a widespread, incurable retrovirus known to cause immunodeficiency and a shortened life span. Despite successful treatment methods, HIV-1 frequently mutates, resulting in antiviral resistance. Many therapies target the HIV-1 protease (PR), which is responsible for cleaving the viral polyprotein essential for its life cycle. HIV-1 PR often evades treatment by way of mutations and less commonly through residue insertions. We have identified a clinical isolate with a five residue insertion between residues 28 and 29. Through molecular dynamics simulations we analyzed the protease protein structure and determined that the residue insertion created a change in the secondary structure of the hinge region of the viral protease. Elucidating the role of insertions could both aid in understanding viral mutations as well as the theoretical effect on patient treatment/outcome.

Section 2: Chikungunya nsP2 Protein Optimization, Purification, Expression and Drug Design

CHAPTER I: INTRODUCTION

1.1 Chikungunya Virus Background:

Chikungunya virus (CHIKV) is a +ssRNA arbovirus belonging to the *Alphavius* genus, and the *Togavirdae* family [35-50]. Chikungunya is considered a neglected tropical disease by the World Health Association (WHO, http://www.who.int/neglected_diseases/diseases/en/), but is becoming a growing concern as an emergent virus to non-tropical climates, resulting from climate change and its consequential global warming, creating an increase in temperatures around the world [50-56]. As an emerging virus, CHIKV may be most notable for severe arthralgia in infected patients spanning from days to years [35-39, 41, 44, 45, 47, 49, 50, 57]. The pain is notoriously agonizing. The name "Chikungunya" is derived from the Makonde language meaning, "that which bends up" which serves as a descriptor of the contorted stance those plagued by severe arthralgia secondary to CHIKV infection exemplify [49, 55, 56, 58]. CHIKV was first identified in East Africa during the 1950s Tanzania outbreak [35, 37, 46, 49, 55, 59], but now affects a minimum of 45 countries spanning the Caribbean, and the Americas [39, 40, 51, 54, 55, 57, 58, 60]. The ability for CHIKV to span many countries is partially due to its mosquito vector. Its spread is additionally due to its capacity to mutate as an RNA virus [35, 40, 49, 59-62]. Originally, vectored by the mosquito *Aedes aegypti*, a mutation created the ability for a second, more aggressive mosquito *Aedes albopictus* to vector and spread the virus [35, 37, 39, 40, 45-47, 49, 52-56, 58, 60-63, 64]. As the climate continues to change, and mutations continue to occur, CHIKV will likely have the capability to continually adapt and spread to new locations. Subsequently, a good understanding of the virus and the viral life cycle is imperative. Furthermore, no FDA drugs are currently approved for the

treatment of CHIKV which garners a need for development of drug therapies and vaccines to prevent the spread of the disease to previously unaffected areas.

1.1.1 Cause:

CHIKV is caused by a mosquito vectored +ssRNA arbovirus [38, 41, 49, 50, 55, 56, 64]. It is a zoonotic virus, passed between humans and non-human primates via mosquito bite [39, 40, 45, 46]. As an RNA virus CHIKV does not have proof-reading capabilities, making it adaptable by way of mutations [62]. Because of its small genome, one point mutation can make a substantial difference in transmission/vector compatibility [35, 40, 49, 59-62].

1.1.2 Viral Mechanism/Protease Significance:

The CHIKV genome is comprised of two open reading frames—one responsible for encoding the nonstructural protein precursor polyprotein, and the second for the encoding of the precursor polyprotein responsible for the three structural proteins [39, 45, 50]. There are four nonstructural proteins: nsp1, nsp2, nsp3, and nsp4 [39, 41, 45, 48]. Structural proteins are responsible for CHIKV viral enzymatic activities. The structural proteins are C (capsid), E1, and E2 (envelope proteins) [39, 41, 45, 48]. These are responsible for non-enzymatic, protective components of the virus. The nonstructural polyprotein is P1234, which is self-cleaved by the protease activity of nsP2 [41, 44-46, 48-50]. The nonstructural proteins, after cleavage, form a replication complex responsible for viral replication [41, 44-46, 48-50, 63]. Each nonstructural protein plays an important role. Nsp1 plays a functional role in attaching the replication complex to the cell membrane, thus acting as an anchor for the complex [41, 45]. Nsp2 has dual roles—cleaving imperative viral nonstructural proteins of the replication complex with its protease and helicase activity. Additionally, the nsp2 plays an active role in evading the host innate immune system by

means of activating the transcription-coupled repair mechanism in the host cell. This repair mechanism destroys polymerase II catalytic subunit, Rbp1, by ubiquitination and degradation. This mechanism also suppresses JAK-STAT signaling pathway in the host cell —both of which are necessary for viral propagation and survival in the host. Additionally, nsp2 has nucleoside triphosphatase (NTPase) and RNA-dependent 5-triphosphatase capabilities [41, 44-49, 63]. Nsp3 functions as cofactor for nsp4 [41] and also acts as part of the replication complex. Aside from its involvement as a cofactor, the function of nsp3 is not fully understood [45]. Lastly, nsp4 is the RNA-dependent RNA polymerase responsible for replication [41, 45, 49]. Because of its essential role in both evasion of the immune system and viral life cycle, nsp2 has been recognized as a promising pharmaceutical target [44-48, 63].

1.2 Clinical Background

1.2.1 Impact/Demographic:

CHIKV was initially isolated in the early 1950s in Tanzania and northern Mozambique [35, 37, 46, 49, 55, 59]. At first it was thought to be a self-limiting tropical virus; however, it has been reported to result in severe complications and fatalities [60, 61]. Throughout the last several decades, CHIKV has continued to spread to new, unaffected regions and is now found in at least 45 countries [39, 40, 51, 57, 58, 60]. Presently, outbreaks cease to be contained to tropical climates. The ability to infect other climates may increase due in part to mutations and infected travelers, as well as climate change potentially influencing the vectors [37, 47, 50, 53, 55].

1.2.2 Symptoms:

CHIKV is characteristically known for the symptom of extreme arthralgia, which can be either acute or chronic [35-39, 41, 44, 45, 47, 49-51, 53, 56, 57, 65]. The name of the CHIKV came from the notorious, severe arthralgia it is known for. Its name means "that which bends up," which describes the contorted posture of an infected patient [49, 55, 56, 58]. The joint pain can be debilitating and has the ability to progress into deforming arthritis [66]. Additionally, chronic arthralgia can occur which can span for over a year post infection [57]. Chronic patients may exhibit high levels of interleukin 6, as well as high levels of granulocyte macrophage colony-stimulating factor without the normal increase in TNF or IL-1b characteristic of other forms of inflammation triggered arthritis [61]. With the ongoing threat of spread due to increases in globalized travel, global warming, and viral mutations facilitating adaption to new vectors [37, 47, 50, 53, 55], rheumatologists are likely to face challenging and unexpected cases of arthralgia due to CHIKV as the virus migrates to more temperate, northern climates.

Normally symptoms are acute in nature, lasting from 3-10 days [50, 57]. Other symptoms associated with CHIKV include an acute onset of high fever, nausea, vomiting, maculopapular rash, myalgia, headache, and chills [35, 36, 39, 41, 44-47, 50, 53-56, 58, 64]. CHIKV patients presenting with Guillain-Barre syndrome and associated neurological symptoms have been reported [67]. Guillain-Barre syndrome is a rare condition, which can progress to troubling symptoms such as flaccid quadriparesis and decreased swallowing and/or breathing capability [67]. Although these symptoms are normally reversible, fatalities can occur due to complications. Initially CHIKV was thought to be a self-limiting illness [39, 51, 53, 61], however, its spread in Reunion Island resulted in 254 reported deaths related either directly or indirectly to CHIKV [61]. With the potential emergence of CHIKV to previously unaffected

areas it is important that medical professionals are prepared to diagnose and treat the condition efficiently. Quick treatment may decrease the likelihood of chronic and debilitating symptoms such as neurological complications, or even death.

1.2.3 Treatment/Prognosis:

No known FDA approved antivirals currently exist [68], although, a recent study conducted a drug screen with potential for berberine, abamectin, and ivermectin (used as anti-insect or anti-parasitic agents, with the potential for wide-spectrum antiviral use). These three agents showed a reduction in viral RNA synthesis, although the mechanism of action is not fully understood [38]. Currently, treatments are focused on alleviating symptoms and inflammation.

1.3 Global Warming and Drug Design Urgency

1.3.1 Global Warming Predictions:

Over the past several decades, atmospheric changes have resulted from an increase in greenhouse gases. Gasses indicated in the atmospheric changes include carbon dioxide, methane, and nitrous oxide [69]. The increase of gasses due to manmade activity, such as fossil fuel combustion, has led to a warming of the earth's surface. [69, 70]. This increase in temperature may facilitate an increase in diseases [69-71]. Viruses vectored by mosquitos, such as CHIKV, present a threat of emergence with climate change as their vectors have the potential to carry out their life cycle in new areas, due to the increased heat, moisture, deforestation, and other ecological changes [55, 69-71]. CHIKV presents a substantial threat of complications to northern climates with naïve populations, who are largely unexposed to the virus [64]. Unaffected

populations have the potential to quickly spread the virus, suffer severe complications, and even potential fatalities, due to exposure [60].

1.3.2 Vectors and Distribution:

CHIKV is primarily vectored by the *Aedes aegypti* and *Aedes albopictus* mosquitos [52-56, 58, 60, 61, 64]. CHIKV underwent a mutation first discovered in the 2006 La Reunion viral outbreak, which created the ability for *Aedes albopictus* to act as a vector [60, 61]. *Aedes albopictus* is capable of spreading the virus to a larger geographical range, due to its ability to survive variable conditions—both rural and urban [52, 55 , 56, 58, 60, 61, 64]. Climate predictions yielded varying results on the outcome for CHIKV vectors due to climate change [72-83]. Although vector predictions vary, it is essential to be prepared as climate change escalates. Furthermore, it is imperative that effective antiviral therapy is available to combat the potential emergence of CHIKV and other vectored viruses in new geographic locations with unaffected, at-risk populations.

1.4 Specific Aims:

The goal of this research is to optimize, express, and purify CHIKV nsP2 protease, with the future direction of small molecule drug design to inhibit nsP2.

1.5 Significance:

Currently there are no known FDA approved CHIKV treatments. CHIKV outbreak is treated by alleviating symptoms, as no known, effective antiviral exists. With the threat of *Arboviral* emergence to unaffected areas of the world, pharmaceutical treatments are imperative.

CHAPTER II: MATERIALS AND METHODS

2.1 Cloning and Small Scale Expression:

Chikungunya virus nsp2 protease (CHIKV) was cloned into a SUMO vector at EZbiolab, inc. (EZBioLab, 2015). A fusion protein was made with a 6x His attached to a SUMO tag, followed by the nsp2 CHIKV sequence with an Ampicillin resistance gene. The clone was transformed into Escherichia coli BL21 Codon Plus (DE3) cells for protein expression.

Protein expression optimization was preformed using 5 mL, small scale cultures. The SUMO tagged CHIKV protein was grown in 5 mL LB medium in the presence of Ampicillin. Protein expression was induced by addition of isopropyl-β-D-thiogalactoside (IPTG). To optimize protein overexpression the following variables were tested: optical density(OD_{600}) prior to induction, IPTG concentration, and temperature. Induction of the cell cultures was carried out at OD_{600} 0.5 or 1.0 with the addition of IPTG at the following concentrations: 0.1mM, 0.5mM, or 1.0mM. Following IPTG induction of the cell culture, protein expression was carried out at either 37°C for three hours or 15°C overnight. After the incubation period the cells were lysed using lysozyme and polyacrylamide gel electrophoresis(SDS-PAGE) (15% w/v polyacrylamide) was used to determine protein expression levels and solubility (**Figure 18**). Results of optimization summarized in **Figure 19**.

Figure 18. Nsp2 Optimization. Protein optimization of CHIKV nsp2. First gel (**top**) tested the OD600 condition. Second set of gels (**middle**) tested IPTG concentration. The third set of gels (**bottom**) tested temperature. Constant conditions are listed and boxed to the left of the corresponding SDS-PAGE gel.

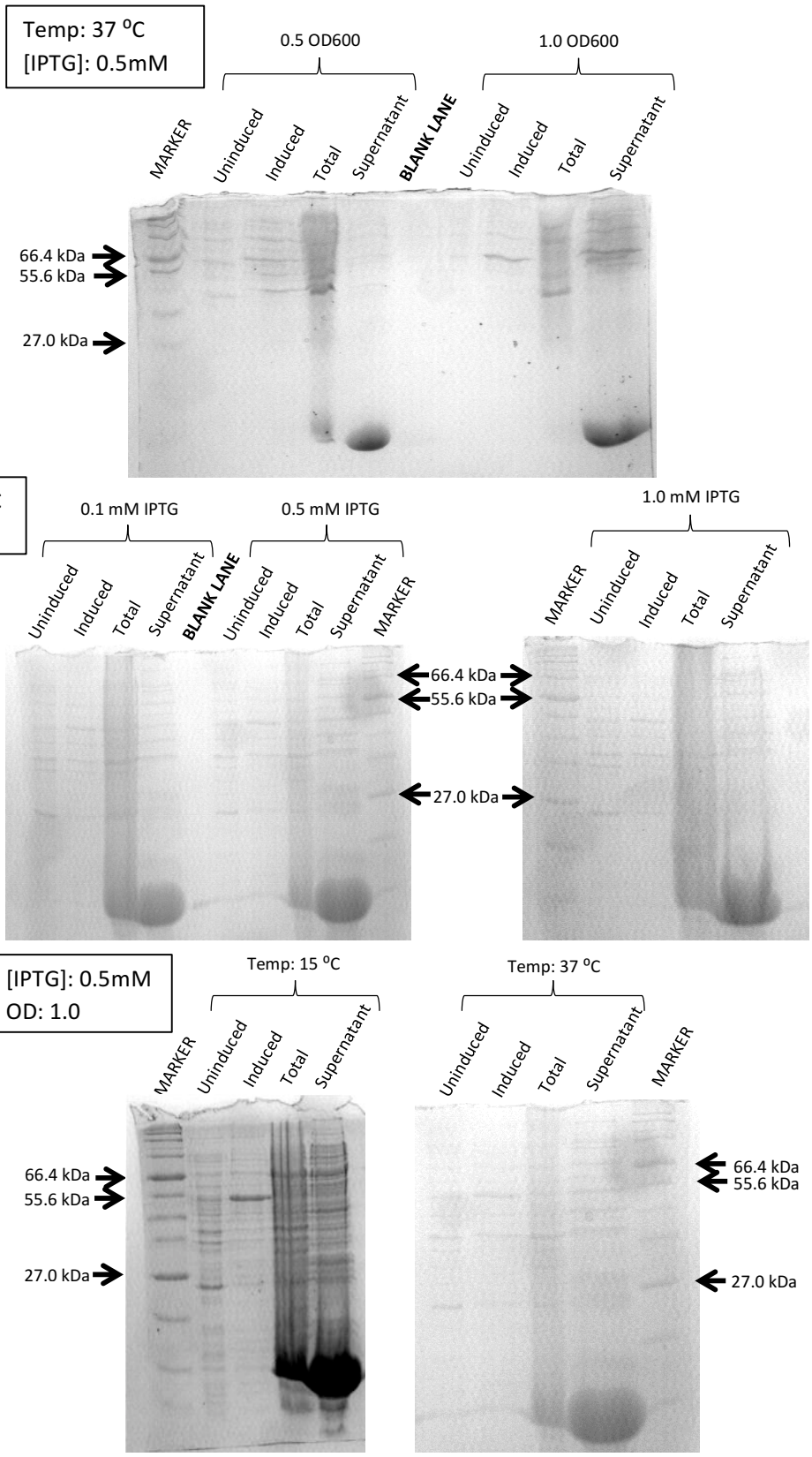

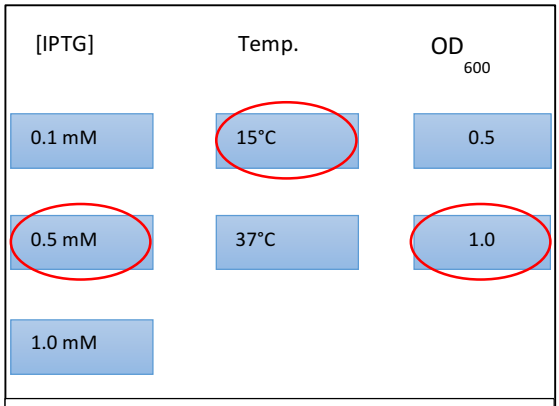

Figure 19. Optimization Results. Summary of optimization results for nsp2. Optimization showed the best temperature is 15°C, IPTG concentration as 0.5mM, and the best OD_{600} as 1.0.

2.2 Large Scale Protein Expression and Purification:

Large scale protein expression was attained using 2 liter cultures. The optimized condition for growth of the cultures was as follows: induction with 0.5mM concentration of IPTG, OD_{600} of 1.0, expression at 15°C overnight. The following day the cells were harvested via centrifugation and lysed by French Press. A Ni^{2+} affinity column (HisTrap™ HP, GE) was used to purify the soluble fraction. The SUMO tag was separated from CHIKV by proteolytic cleavage of the His6-SUMO tag with yeast SUMO Protease 1 after the elution of the fractions. The cleaved protein was subjected to an additional round of Ni^{2+} purification followed by size-exclusion chromatography (Superdex 200, GE). Purified CHIKV was collected and concentrated to ~19 mg/mL. The accuracy of the purified protein in the elution fractions were tested using SDS-PAGE (15% w/v polyacrylamide). The gels were used to analyze the filtrate based on size and Coomassie Brilliant Blue staining was used to visualize the protein bands.

2.3 Characterization of Enzyme Activity

FRET-based fluorometric enzyme assay was used to test the enzymatic activity of CHIKV. CHIKV was diluted in reaction buffer containing Tris 50mM, NaCl 10mM, at a pH of 9.1 to a final concentration of 539 nM. The reaction was initiated by adding FRET substrate (AnaSpec Inc.). The substrate used is based on the P4-P5' residues of the nsp1/nsp2 (residues RAGAGIEK), nsp2/nsp3 (RAGCAPSYK), and nsp3/nsp4 (RAGGYIFSK) cleavage sites. The FRET substrate was serially diluted from concentrations of 100 µM to 39 nM and 75µM to 37.5µM then added to the reaction to determine the kinetic parameters. The final reaction volume within the well was 100 µL. A microplate reader (SpectraMax M5, Molecular Devices, Sunnyvale, CA, USA) was responsible for monitoring the fluorescence emitted by substrate

cleavage at 488 nm excitation wavelength with an emission wavelength of 520 nm. The reaction was performed at 37°C with readings taken every minute for a total duration of 21 minutes. Standard curves were created, data was plotted and analyzed using GraphPad Prism v. 6.07.

CHAPTER III: RESULTS

3.1 Overexpression and Purification of CHIKV Protease:

Using the optimized overexpression conditions outlined in section 2.1, a 2 liter culture of E. coli was used to overexpress CHIKV. The resulting cells were collected via centrifugation and lysed by French press, **Figure 20** [1]shows a flowchart representing the order in which purification occurred. Expressed SUMO-CHIKV fusion protein is seen at ~ 55.6 kDa molecular weight on a 15% v/w polyacrylamide SDS-PAGE gel as shown in **Figure 21**. The first Ni^{2+} column was applied with the elution of SUMO-CHIKV protein as a result of an imidazole gradient. **Figure 21** shows the results from the first Ni^{2+} column as well as the desalting column, visualized on SDS-PAGE. The elution fractions B1-B6 were cleaved by yeast SUMO protease to remove the SUMO tag from CHIKV prior to the second Ni^{2+} purification. CHIKV was eluted from second a Ni^{2+} column as seen in **Figure 22**. Partial ULP cleavage was observed, and SDS-

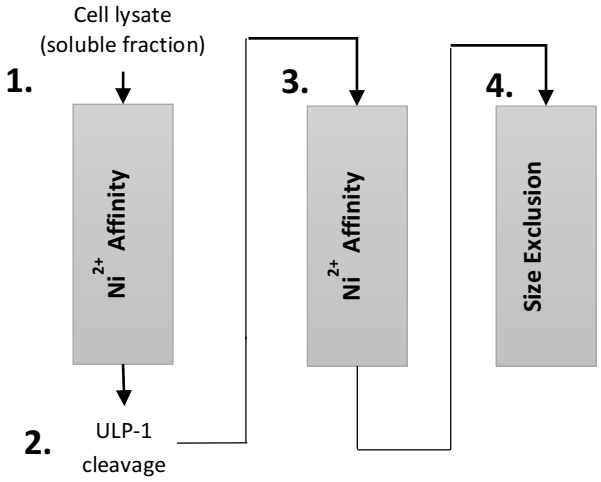

Figure 20. Protein Purification Scheme [1]. Purification was accomplished through two Ni^{2+} affinity columns (with ULP-1 cleavage of SUMO between), and subsequent Size Exclusion chromatography.

PAGE showed three protein bands. CHIKV is expected to present with the molecular weight of 37.4kDa, but bands were displayed at the experimental molecular weight of ~55.6kDa, ~35kDa, and ~19kDa on SDS-PAGE gel as seen in figure D. These results indicate partial ULP-1 cleavage, resulting in fusion protein, nsp2, and SUMO protein, respectively.

A final round of purification was obtained using size-exclusion chromatography. A strong, symmetrical peek is seen at ~86 mL indicting the beginning of CHIKV elution. The symmetrical peak indicates successful protein purification representative of only one species (**Figure 23**). Fractions D3-D12 were concentrated to ~19mg/mL.

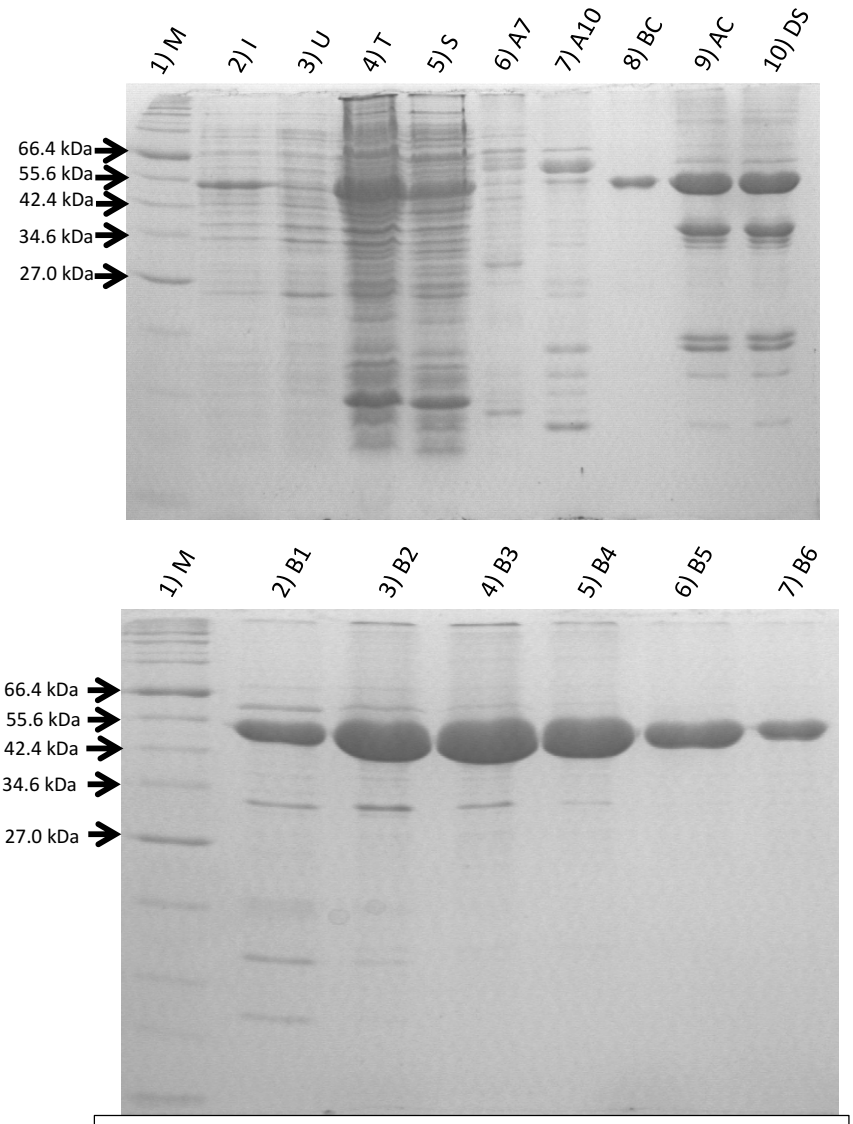

Figure 21. Optimization, First Nickel Column, and Desalting Column. (**Top**) SDS-PAGE gel containing the following: lane 1: marker; lane 2: induced; lane 3: uninduced; lane 4: total, lane 5: supernatant; lane 6 & 7: fractions after first Ni^{2+} column; Lanes 8 & 9: before/after ULP cleavage; lane 10: desalt column. Protein is soluble, but incomplete ULP cleavage is observed. (**Bottom**) SDS-PAGE gel containing the following: lane 1: marker; lanes 2-7: 1st Ni^{2+} column elution fractions; lanes 8-10 blank.

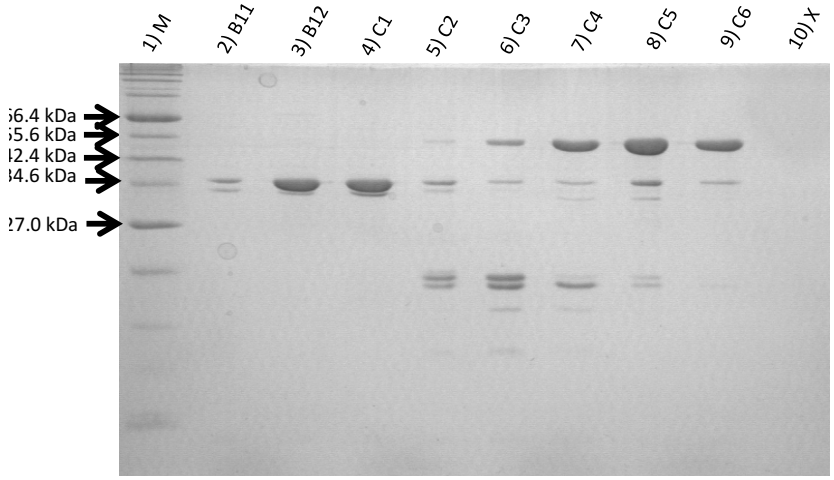

3.2 Characterization of Enzyme Activity

FRET based assays were used to test enzymatic activity of purified CHIKV as described in section 2.3. Each substrate was tested to determine enzyme activity in the presence and absence of DTT in relation to the following cleavage sites (residues P4-P5'): nsp1/nsp2, nsp2/nsp3, and nsp3/nsp4. Each peptide contained a fluorescent tag (Hilyte Fluor ™, AnaSpec, Inc.) on the N-terminus of the P4 Arginine. The enzyme optimization data is shown in **Figure 24** as relative fluorescent units (RFU) as a function of enzyme

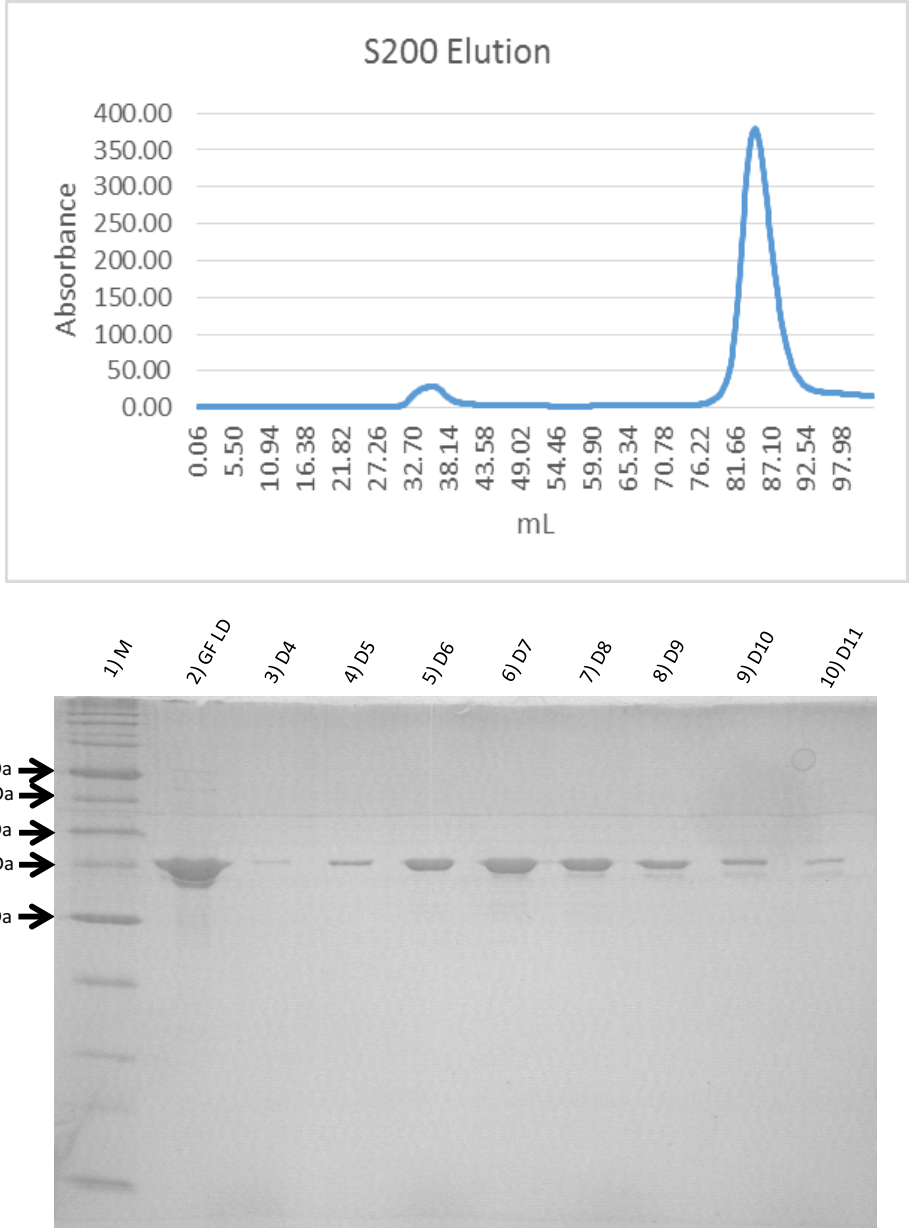

Figure 23. Size-exclusion Elution. Results for the size exclusion elution. The sample shows a symmetric peak (**top**) when measuring the absorbance vs mL of sample, and one protein band (**bottom**) in SDS-PAGE gel, indicating successful purification of CHIKV nsp2. The lanes of the SDS-PAGE are as follows: lane 1: marker; lane 2: gel load; lanes 3-10: size-exclusion elution

concentration. The nsp1/nsp2 cleavage site showed the highest RFU (~0.3 RFU) without DTT at ~256nM enzyme concentration. The nsp2/nsp3 cleavage site showed similar RFU values with and without DTT. The highest nsp2/nsp3 RFU (~0.25) was seen with DTT at ~512nM enzyme concentration. The nsp3/nsp4 did not show activity.

Figure 24. Enzyme Activity Assay. Enzyme optimization assay results measured as a function of RFU as a function of enzyme concentration. Results recorded without (**top**) and with (**bottom**) DTT.

CHAPTER IV: CONCLUSIONS AND DISCUSSIONS

4.1 Overview:

Expression, purification, and characterization of CHIKV was successful, yielding ~19 mg/mL or purified protein. The kinetic assays confirmed activity of CHIKV nsp2, further studies will

aim at elucidating accurate binding information, as well as small molecule drug design.

4.2 Key Findings:

CHIKV appears to have an affinity for the gels used in purification. It is possible that this is due to ribose binding, as nsp2 is involved in the formation of the replication complex, and due to its NTPase activity, which provides energy for its helicase activity [41]. Additionally, when optimizing the protein, we found that it expresses best at lower temperatures (15 ^{o}C). This may be in part due to its association with the replication complex docked to the cytosolic cell membrane [41]. The kinetic assays show enzymatic activity, creating the potential to test drug targets with nsp2, active protease.

4.3 Concluding Remarks:

In summary, we successfully optimized, expressed, and purified CHIKV nsp2 and conducted enzyme characterization assays which validated the enzymes activity. No FDA approved treatments currently exist for CHIKV, but with the threat of an *Arborviral* migration to previously unaffected climates due to global warming and other globalization factors, drug design to inhibit fundamental portions of the viral cycle is imperative. Future studies will aim to conduct drug screens and to crystalize wildtype CHIKV to yield accurate results for potential small molecule protease inhibitors.

Abstract:

Chikungunya virus (CHIKV) is an incurable *Arbovirus* creating the most notable symptom of severe and sometimes chronic arthralgia. CHIKV is considered a neglected tropical virus by the World Health Association (WHO), with the potential of becoming a larger scale threat in part due to the influence of global warming on the mosquito population that serve as vectors for CHIKV. The virus has a life cycle is dependent on its nonstructural protein function, one of specific interest is nsP2. We have successfully expressed, optimized, and purified active CHIKV nsP2. Future studies will look at small peptidomimetic drug design.

References

[1] Kuiper, B.D., Slater, K., Spellmon, N., Holcomb, J., Medapureddy, P., Muzzarelli, K.M., et al. Increased activity of unlinked Zika virus NS2B/NS3 protease compared to linked Zika virus protease. Biochem Biophys Res Commun. 2017.
[2] Liu, Z., Huang, X., Hu, L., Pham, L., Poole, K.M., Tang, Y., et al. Effects of Hinge-region Natural Polymorphisms on Human Immunodeficiency Virus-Type 1 Protease Structure, Dynamics, and Drug Pressure Evolution. J Biol Chem. 2016, 291, 22741-56.
[3] Chow, A., Tey, J., Win, M.K., Leo, Y.S. Causes of death and factors associated with early death among human immunodeficiency virus (HIV)-infected persons in Singapore: pre-highly active antiretroviral therapy (HAART) and Peri-HAART. Ann Acad Med Singapore. 2012, 41, 563-70.
[4] Bandaranayake, R.M., Kolli, M., King, N.M., Nalivaika, E.A., Heroux, A., Kakizawa, J., et al. The effect of clade-specific sequence polymorphisms on HIV-1 protease activity and inhibitor resistance pathways. J Virol. 2010, 84, 9995-10003.
[5] Wlodawer, A., Miller, M., Jaskolski, M., Sathyanarayana, B.K., Baldwin, E., Weber, I.T., et al. Conserved folding in retroviral proteases: crystal structure of a synthetic HIV-1 protease. Science. 1989, 245, 616-21.
[6] Liu, Z., Wang, Y., Brunzelle, J., Kovari, I.A., Kovari, L.C. Nine crystal structures determine the substrate envelope of the MDR HIV-1 protease. Protein J. 2011, 30, 173-83.
[7] Sayer, J.M., Agniswamy, J., Weber, I.T., Louis, J.M. Autocatalytic maturation, physical/chemical properties, and crystal structure of group N HIV-1 protease: relevance to drug resistance. Protein Sci. 2010, 19, 2055-72.
[8] Bannwarth, L., Rose, T., Dufau, L., Vanderesse, R., Dumond, J., Jamart-Gregoire, B., et al. Dimer disruption and monomer sequestration by alkyl tripeptides are successful strategies for inhibiting wild-type and multidrug-resistant mutated HIV-1 proteases. Biochemistry. 2009, 48, 379-87.
[9] Meher, B.R., Wang, Y. Exploring the drug resistance of V32I and M46L mutant HIV-1 protease to inhibitor TMC114: flap dynamics and binding mechanism. J Mol Graph Model. 2015, 56, 60-73.
[10] Yu, Y., Wang, J., Shao, Q., Shi, J., Zhu, W. Effects of drug-resistant mutations on the dynamic properties of HIV-1 protease and inhibition by Amprenavir and Darunavir. Sci Rep. 2015, 5, 10517.
[11] Louis, J.M., Roche, J. Evolution under Drug Pressure Remodels the Folding Free-Energy Landscape of Mature HIV-1 Protease. J Mol Biol. 2016, 428, 2780-92.
[12] Agniswamy, J., Shen, C.H., Aniana, A., Sayer, J.M., Louis, J.M., Weber, I.T. HIV-1 protease with 20 mutations exhibits extreme resistance to clinical inhibitors through coordinated structural rearrangements. Biochemistry. 2012, 51, 2819-28.
[13] Andersson, H.O., Fridborg, K., Lowgren, S., Alterman, M., Muhlman, A., Bjorsne, M., et al. Optimization of P1-P3 groups in symmetric and asymmetric HIV-1 protease inhibitors. Eur J Biochem. 2003, 270, 1746-58.
[14] Silva, A.M., Cachau, R.E., Sham, H.L., Erickson, J.W. Inhibition and catalytic mechanism of HIV-1 aspartic protease. J Mol Biol. 1996, 255, 321-46.
[15] Cai, Y., Myint, W., Paulsen, J.L., Schiffer, C.A., Ishima, R., Kurt Yilmaz, N. Drug Resistance Mutations Alter Dynamics of Inhibitor-Bound HIV-1 Protease. J Chem Theory Comput. 2014, 10, 3438-48.
[16] Nair, A.C., Miertus, S., Tossi, A., Romeo, D. A computational study of the resistance of HIV-1 aspartic protease to the inhibitors ABT-538 and VX-478 and design of new analogues. Biochem Biophys Res Commun. 1998, 242, 545-51.

[17] Kim, E.Y., Winters, M.A., Kagan, R.M., Merigan, T.C. Functional correlates of insertion mutations in the protease gene of human immunodeficiency virus type 1 isolates from patients. J Virol. 2001, 75, 11227-33.
[18] Ding, F., Layten, M., Simmerling, C. Solution structure of HIV-1 protease flaps probed by comparison of molecular dynamics simulation ensembles and EPR experiments. J Am Chem Soc. 2008, 130, 7184-5.
[19] Nakashima, M., Ode, H., Suzuki, K., Fujino, M., Maejima, M., Kimura, Y., et al. Unique Flap Conformation in an HIV-1 Protease with High-Level Darunavir Resistance. Front Microbiol. 2016, 7, 61.
[20] Appadurai, R., Senapati, S. Dynamical Network of HIV-1 Protease Mutants Reveals the Mechanism of Drug Resistance and Unhindered Activity. Biochemistry. 2016, 55, 1529-40.
[21] Petropoulos, C.J., Parkin, N.T., Limoli, K.L., Lie, Y.S., Wrin, T., Huang, W., et al. A novel phenotypic drug susceptibility assay for human immunodeficiency virus type 1. Antimicrob Agents Chemother. 2000, 44, 920-8.
[22] Cunningham, S., Ank, B., Lewis, D., Lu, W., Wantman, M., Dileanis, J.A., et al. Performance of the applied biosystems ViroSeq human immunodeficiency virus type 1 (HIV-1) genotyping system for sequence-based analysis of HIV-1 in pediatric plasma samples. J Clin Microbiol. 2001, 39, 1254-7.
[23] Biasini, M., Bienert, S., Waterhouse, A., Arnold, K., Studer, G., Schmidt, T., et al. SWISS-MODEL: modelling protein tertiary and quaternary structure using evolutionary information. Nucleic Acids Res. 2014, 42, W252-8.
[24] Kiefer, F., Arnold, K., Kunzli, M., Bordoli, L., Schwede, T. The SWISS-MODEL Repository and associated resources. Nucleic Acids Res. 2009, 37, D387-92.
[25] Arnold, K., Bordoli, L., Kopp, J., Schwede, T. The SWISS-MODEL workspace: a web-based environment for protein structure homology modelling. Bioinformatics. 2006, 22, 195-201.
[26] Guex, N., Peitsch, M.C., Schwede, T. Automated comparative protein structure modeling with SWISS-MODEL and Swiss-PdbViewer: a historical perspective. Electrophoresis. 2009, 30 Suppl 1, S162-73.
[27] Muzammil, S., Armstrong, A.A., Kang, L.W., Jakalian, A., Bonneau, P.R., Schmelmer, V., et al. Unique thermodynamic response of tipranavir to human immunodeficiency virus type 1 protease drug resistance mutations. J Virol. 2007, 81, 5144-54.
[28] Humphrey, W., Dalke, A., Schulten, K. VMD: visual molecular dynamics. J Mol Graph. 1996, 14, 33-8, 27-8.
[29] Phillips, J.C., Braun, R., Wang, W., Gumbart, J., Tajkhorshid, E., Villa, E., et al. Scalable molecular dynamics with NAMD. J Comput Chem. 2005, 26, 1781-802.
[30] Best, R.B., Zhu, X., Shim, J., Lopes, P.E., Mittal, J., Feig, M., et al. Optimization of the additive CHARMM all-atom protein force field targeting improved sampling of the backbone phi, psi and side-chain chi(1) and chi(2) dihedral angles. J Chem Theory Comput. 2012, 8, 3257-73.
[31] Dewdney, T.G., Wang, Y., Kovari, I.A., Reiter, S.J., Kovari, L.C. Reduced HIV-1 integrase flexibility as a mechanism for raltegravir resistance. J Struct Biol. 2013, 184, 245-50.
[32] Salisburg, A.M., Deline, A.L., Lexa, K.W., Shields, G.C., Kirschner, K.N. Ramachandran-type plots for glycosidic linkages: Examples from molecular dynamic simulations using the Glycam06 force field. J Comput Chem. 2009, 30, 910-21.
[33] Soares, R.O., Torres, P.H., da Silva, M.L., Pascutti, P.G. Unraveling HIV protease flaps dynamics by Constant pH Molecular Dynamics simulations. J Struct Biol. 2016, 195, 216-26.
[34] Jordan, P.S., Poon, A., Eron, J., Squires, K., Ignacio, C., Richman, D.D., et al. A novel codon insert in protease of clade B HIV type 1. AIDS Res Hum Retroviruses. 2009, 25, 547-50.
[35] Carrera, J.P., Diaz, Y., Denis, B., Barahona de Mosca, I., Rodriguez, D., Cedeno, I., et al. Unusual pattern of chikungunya virus epidemic in the Americas, the Panamanian experience. PLoS Negl Trop Dis. 2017, 11, e0005338.

[36] Pastula, D.M., Hancock, W.T., Bel, M., Biggs, H., Marfel, M., Lanciotti, R., et al. Chikungunya virus disease outbreak in Yap State, Federated States of Micronesia. PLoS Negl Trop Dis. 2017, 11, e0005410.
[37] Tsetsarkin, K.A., Chen, R., Weaver, S.C. Interspecies transmission and chikungunya virus emergence. Curr Opin Virol. 2016, 16, 143-50.
[38] Varghese, F.S., Kaukinen, P., Glasker, S., Bespalov, M., Hanski, L., Wennerberg, K., et al. Discovery of berberine, abamectin and ivermectin as antivirals against chikungunya and other alphaviruses. Antiviral Res. 2016, 126, 117-24.
[39] Agarwal, A., Dash, P.K., Singh, A.K., Sharma, S., Gopalan, N., Rao, P.V., et al. Evidence of experimental vertical transmission of emerging novel ECSA genotype of Chikungunya Virus in Aedes aegypti. PLoS Negl Trop Dis. 2014, 8, e2990.
[40] Tsetsarkin, K.A., Weaver, S.C. Sequential adaptive mutations enhance efficient vector switching by Chikungunya virus and its epidemic emergence. PLoS Pathog. 2011, 7, e1002412.
[41] Bourai, M., Lucas-Hourani, M., Gad, H.H., Drosten, C., Jacob, Y., Tafforeau, L., et al. Mapping of Chikungunya virus interactions with host proteins identified nsP2 as a highly connected viral component. J Virol. 2012, 86, 3121-34.
[42] Leung, J.Y., Ng, M.M., Chu, J.J. Replication of alphaviruses: a review on the entry process of alphaviruses into cells. Adv Virol. 2011, 2011, 249640.
[43] Thomas, S., Rai, J., John, L., Schaefer, S., Putzer, B.M., Herchenroder, O. Chikungunya virus capsid protein contains nuclear import and export signals. Virol J. 2013, 10, 269.
[44] Ramakrishnan, C., Kutumbarao, N.H., Suhitha, S., Velmurugan, D. Structure-function relationship of Chikungunya nsP2 protease: A comparative study with papain. Chem Biol Drug Des. 2016.
[45] Fros, J.J., Pijlman, G.P. Alphavirus Infection: Host Cell Shut-Off and Inhibition of Antiviral Responses. Viruses. 2016, 8.
[46] Saisawang, C., Sillapee, P., Sinsirimongkol, K., Ubol, S., Smith, D.R., Ketterman, A.J. Full length and protease domain activity of chikungunya virus nsP2 differ from other alphavirus nsP2 proteases in recognition of small peptide substrates. Biosci Rep. 2015, 35.
[47] Bao, H., Ramanathan, A.A., Kawalakar, O., Sundaram, S.G., Tingey, C., Bian, C.B., et al. Nonstructural protein 2 (nsP2) of Chikungunya virus (CHIKV) enhances protective immunity mediated by a CHIKV envelope protein expressing DNA Vaccine. Viral Immunol. 2013, 26, 75-83.
[48] Akhrymuk, I., Kulemzin, S.V., Frolova, E.I. Evasion of the innate immune response: the Old World alphavirus nsP2 protein induces rapid degradation of Rpb1, a catalytic subunit of RNA polymerase II. J Virol. 2012, 86, 7180-91.
[49] Fros, J.J., Liu, W.J., Prow, N.A., Geertsema, C., Ligtenberg, M., Vanlandingham, D.L., et al. Chikungunya virus nonstructural protein 2 inhibits type I/II interferon-stimulated JAK-STAT signaling. J Virol. 2010, 84, 10877-87.
[50] Pohjala, L., Utt, A., Varjak, M., Lulla, A., Merits, A., Ahola, T., et al. Inhibitors of alphavirus entry and replication identified with a stable Chikungunya replicon cell line and virus-based assays. PLoS One. 2011, 6, e28923.
[51] Pineda, C., Munoz-Louis, R., Caballero-Uribe, C.V., Viasus, D. Chikungunya in the region of the Americas. A challenge for rheumatologists and health care systems. Clin Rheumatol. 2016, 35, 2381-5.
[52] Roiz, D., Bousses, P., Simard, F., Paupy, C., Fontenille, D. Autochthonous Chikungunya Transmission and Extreme Climate Events in Southern France. PLoS Negl Trop Dis. 2015, 9, e0003854.
[53] Yactayo, S., Staples, J.E., Millot, V., Cibrelus, L., Ramon-Pardo, P. Epidemiology of Chikungunya in the Americas. J Infect Dis. 2016, 214, S441-S5.
[54] Kuri-Morales, P.A., Guzman-Morales, E., De La Paz-Nicolau, E., Salas-Fernandez, A. [Emerging and reemerging diseases]. Gac Med Mex. 2015, 151, 674-80.

[55] Waldock, J., Chandra, N.L., Lelieveld, J., Proestos, Y., Michael, E., Christophides, G., et al. The role of environmental variables on Aedes albopictus biology and chikungunya epidemiology. Pathog Glob Health. 2013, 107, 224-41.
[56] Weber, C., Konig, R., Niedrig, M., Emmerich, P., Schnierle, B.S. A neutralization assay for chikungunya virus infections in a multiplex format. J Virol Methods. 2014, 201, 7-12.
[57] Feldstein, L.R., Rowhani-Rahbar, A., Staples, J.E., Weaver, M.R., Halloran, M.E., Ellis, E.M. Persistent Arthralgia Associated with Chikungunya Virus Outbreak, US Virgin Islands, December 2014-February 2016. Emerg Infect Dis. 2017, 23, 673-6.
[58] Gutierrez-Saravia, E., Gutierrez, C.E. Chikungunya Virus in the Caribbean: A Threat for All of the Americas. J Pediatric Infect Dis Soc. 2015, 4, 1-3.
[59] Christofferson, R.C., Chisenhall, D.M., Wearing, H.J., Mores, C.N. Chikungunya viral fitness measures within the vector and subsequent transmission potential. PLoS One. 2014, 9, e110538.
[60] Chikungunya disease: gaps and opportunities in public health and research in the Americas. Wkly Epidemiol Rec. 2015, 90, 571-6.
[61] Madariaga, M., Ticona, E., Resurrecion, C. Chikungunya: bending over the Americas and the rest of the world. Braz J Infect Dis. 2016, 20, 91-8.
[62] Arias-Goeta, C., Moutailler, S., Mousson, L., Zouache, K., Thiberge, J.M., Caro, V., et al. Chikungunya virus adaptation to a mosquito vector correlates with only few point mutations in the viral envelope glycoprotein. Infect Genet Evol. 2014, 24, 116-26.
[63] Mathur, K., Anand, A., Dubey, S.K., Sanan-Mishra, N., Bhatnagar, R.K., Sunil, S. Analysis of chikungunya virus proteins reveals that non-structural proteins nsP2 and nsP3 exhibit RNA interference (RNAi) suppressor activity. Sci Rep. 2016, 6, 38065.
[64] Diaz-Gonzalez, E.E., Kautz, T.F., Dorantes-Delgado, A., Malo-Garcia, I.R., Laguna-Aguilar, M., Langsjoen, R.M., et al. First Report of Aedes aegypti Transmission of Chikungunya Virus in the Americas. Am J Trop Med Hyg. 2015, 93, 1325-9.
[65] Scully, C., Samaranayake, L.P. Emerging and changing viral diseases in the new millennium. Oral Dis. 2016, 22, 171-9.
[66] Vijayan, V., Sukumaran, S. Chikungunya Virus Disease: An Emerging Challenge for the Rheumatologist. J Clin Rheumatol. 2016, 22, 203-11.
[67] Agarwal, A., Vibha, D., Srivastava, A.K., Shukla, G., Prasad, K. Guillain-Barre syndrome complicating chikungunya virus infection. J Neurovirol. 2017.
[68] Nawas, Z.Y., Tong, Y., Kollipara, R., Peranteau, A.J., Woc-Colburn, L., Yan, A.C., et al. Emerging infectious diseases with cutaneous manifestations: Viral and bacterial infections. J Am Acad Dermatol. 2016, 75, 1-16.
[69] Rossati, A. Global Warming and Its Health Impact. Int J Occup Environ Med. 2017, 8, 7-20.
[70] Barrett, B., Charles, J.W., Temte, J.L. Climate change, human health, and epidemiological transition. Prev Med. 2015, 70, 69-75.
[71] Shope, R. Global climate change and infectious diseases. Environ Health Perspect. 1991, 96, 171-4.
[72] Escobar, L.E., Romero-Alvarez, D., Leon, R., Lepe-Lopez, M.A., Craft, M.E., Borbor-Cordova, M.J., et al. Declining Prevalence of Disease Vectors Under Climate Change. Sci Rep. 2016, 6, 39150.
[73] Cunze, S., Kochmann, J., Koch, L.K., Klimpel, S. Aedes albopictus and Its Environmental Limits in Europe. PLoS One. 2016, 11, e0162116.
[74] Equihua, M., Ibanez-Bernal, S., Benitez, G., Estrada-Contreras, I., Sandoval-Ruiz, C.A., Mendoza-Palmero, F.S. Establishment of Aedes aegypti (L.) in mountainous regions in Mexico: Increasing number of population at risk of mosquito-borne disease and future climate conditions. Acta Trop. 2017, 166, 316-27.
[75] Lima-Camara, T.N. Emerging arboviruses and public health challenges in Brazil. Rev Saude Publica. 2016, 50.

[76] Koch, L.K., Cunze, S., Werblow, A., Kochmann, J., Dorge, D.D., Mehlhorn, H., et al. Modeling the habitat suitability for the arbovirus vector Aedes albopictus (Diptera: Culicidae) in Germany. Parasitol Res. 2016, 115, 957-64.
[77] Ogden, N.H., Milka, R., Caminade, C., Gachon, P. Recent and projected future climatic suitability of North America for the Asian tiger mosquito Aedes albopictus. Parasit Vectors. 2014, 7, 532.
[78] Rochlin, I., Ninivaggi, D.V., Hutchinson, M.L., Farajollahi, A. Climate change and range expansion of the Asian tiger mosquito (Aedes albopictus) in Northeastern USA: implications for public health practitioners. PLoS One. 2013, 8, e60874.
[79] Smith, C.D., Freed, T.Z., Leisnham, P.T. Prior Hydrologic Disturbance Affects Competition between Aedes Mosquitoes via Changes in Leaf Litter. PLoS One. 2015, 10, e0128956.
[80] Alto, B.W., Juliano, S.A. Precipitation and temperature effects on populations of Aedes albopictus (Diptera: Culicidae): implications for range expansion. J Med Entomol. 2001, 38, 646-56.
[81] Adelman, Z.N., Anderson, M.A., Wiley, M.R., Murreddu, M.G., Samuel, G.H., Morazzani, E.M., et al. Cooler temperatures destabilize RNA interference and increase susceptibility of disease vector mosquitoes to viral infection. PLoS Negl Trop Dis. 2013, 7, e2239.
[82] Thongsripong, P., Green, A., Kittayapong, P., Kapan, D., Wilcox, B., Bennett, S. Mosquito vector diversity across habitats in central Thailand endemic for dengue and other arthropod-borne diseases. PLoS Negl Trop Dis. 2013, 7, e2507.
[83] Samy, A.M., Elaagip, A.H., Kenawy, M.A., Ayres, C.F., Peterson, A.T., Soliman, D.E. Climate Change Influences on the Global Potential Distribution of the Mosquito Culex quinquefasciatus, Vector of West Nile Virus and Lymphatic Filariasis. PLoS One. 2016, 11, e0163863.